CHAPTER III
RESULTS AND DISCUSSION

3.1 Regime Identification of HDPE, LLDPE and MDPE

In this study we employed two LLDPE's (L2009F, L2020F), MDPE (M3204RU) and three HDPE's (N3260, H5690S and R1760) of different molecular weights as listed in Table 3.1 below, because sharkskin defects occur from these materials.

Table 3.1 Molecular weights of HDPE, LDPE, LLDPE, MDPE and PP studies

Materials	Company	M_w (g/mol)	M_n (g/mol)	M_w/M_n	sharkskin defects
HDPE					
H5604F	TPE	1.33×10^5	2,249	59.14	no sharkskin
H5840B	TPE	1.22×10^5	10,140	12.03	no sharkskin
H6430BM	TPE	1.20×10^5	10,100	11.88	no sharkskin
N3260	TPI	1.92×10^4	9,812	1.96	sharkskin
H5690S	TPI	1.84×10^4	9,780	1.88	sharkskin
R1760	TPI	1.36×10^4	8,214	1.86	sharkskin
H6205JU	TPE	9.82×10^4	7,314	13.43	no sharkskin
H5818J	TPE	5.71×10^4	2,617	21.82	no sharkskin
LDPE					
LD2130F	TPE	9.23×10^4	13,012	7.09	no sharkskin
LD1708J	TPE	8.14×10^4	10,823	7.52	no sharkskin
LD1630J	TPE	8.40×10^4	7,589	11.07	no sharkskin
LLDPE, MDPE					
L2009F	TPE	1.03×10^5	5,132	17.11	sharkskin
L2020F	TPE	6.07×10^4	4,492	13.51	sharkskin
M3204RU	TPE	3.36×10^4	3,723	9.02	sharkskin
PP					
P340J	TPE	1.88×10^5	33,387	5.63	no sharkskin
P640J	TPE	1.19×10^5	24,387	4.88	no sharkskin
P740J	TPE	1.02×10^5	19,568	5.21	no sharkskin

3.1.1 Flow curves

Flow curve is the plot of the wall shear stress (τ_w) versus apparent strain rate ($\dot{\gamma}_a$) as obtained by the capillary rheometer. In each flow curve, the testing temperature was set at 190 °C. We divided the flow curve into at least four regimes, according to the type of the flow behaviour and the appearances of extrudate surfaces, in order to be consistent with a published literature (*Kalika and Denn, 1987*). The flow curves of LLDPE (L2009F, L2020F), MDPE (M3204RU) and HDPE (N3260, H5690S, R1760) for the smaller capillary, l_c = 22.5 mm and d_c = 0.7645 mm (die no. 614), are shown in Figure 3.2a - Figure 3.2f. The results can be summarized as follow.

Regime I corresponds to smooth to semi-smooth extrudate skins, this regime produces various melt extrudate skins: glossy smooth, loss of gloss or matte. The flow is steady.

Regime II was determined from the onset of a sharkskin extrudate. A sharkskin surface is generally refered to a surface roughness that modulates the extrudate diameter by no more than one percent or so (*Larson 1992*). Sharkskin consists of semiregular cracks or grooves that run mainly perpendicular to the flow axis. The *Regime II* can be separated from the *Regime I* by the appearance of a sharkskin surface, which has skin roughness of high frequency but with some order [Figure 3.2 (b)]. Sharkskin is the first form of surface distortion encountered with increasing shear rate. The onset of sharkskin is indicated by a distinct change in the slope of the flow curve (*Kurtz, 1984*, *Ramamurthy, 1986*). Our results indicate that the critical wall shear stress falls in the range 2.24×10^6 - 3.72×10^6 dynes/cm^2 (the results listed in Table 3.3), consistent with a previous study which observed the critical wall shear stress to be in the range 2.6×10^6 - 4.3×10^6 dynes/cm^2 for sharkskin defects (*Kalika and Denn, 1987*). It is in this regime that the physics of

adhesion between the polymer and the metal surface dominates the macroscopic behavior. The adhesive process of melt and the influence on the conformation of polymer near the surface is an area that has received little attention until recently. Sharkskin defect has been suggested to originate from an *unsteady* hydrodynamic boundary condition (HBC) at the die rim as the LLDPE departs the die either in a stick state or in a slip state caused by a local entanglement-to-disentanglement transition (*Wang, Drda and Young-Woo Inn, 1996*).

Regime III is an oscillating flow regime. Here, the stress becomes double valued, and the extrudate alternates in periodic fashion between a sharkskin and a smooth surface section. This is a result of the wall slip and stick at the die-melt interface, similar to the behaviors observed in a constant force mode capillary (*Wang and Drda, 1996*). It can be argued that as the wall shear stress reaches a critical value, chains near the wall begin to disentangle and a thin layer of disentanglement develops where the wall slip occurs; the force required to push the plunger decreases. As chains relax, the disentaglement layer disappears and the melt begins to adhere to the wall again; the force required to move the plunger must compensate and increase. We observed that the melt extrudate exited the die at fluctuating volume flow rate. The skin texture of extrudate in *Regime III* has two alternating sections: smooth, glossy surface (corresponding to 'slipping') when the load increases and a rough, sharkskin surface (corresponding to 'sticking') when the load descends. (*Kalika and Denn, 1987*).

Regime IV is the melt fracture regime. Melt fracture is identified when the roughness amplitude is above 5-10% and no ordered appearence can be observed (*Petrie and Denn 1976, Denn 1990, Larson 1992*).

The flow curves of LLDPE (L2009F, L2020F), MDPE (M3204RU) and HDPE (N3260, H5690S, R1760) are shown in Figure 3.1a - Figure 3.1f.

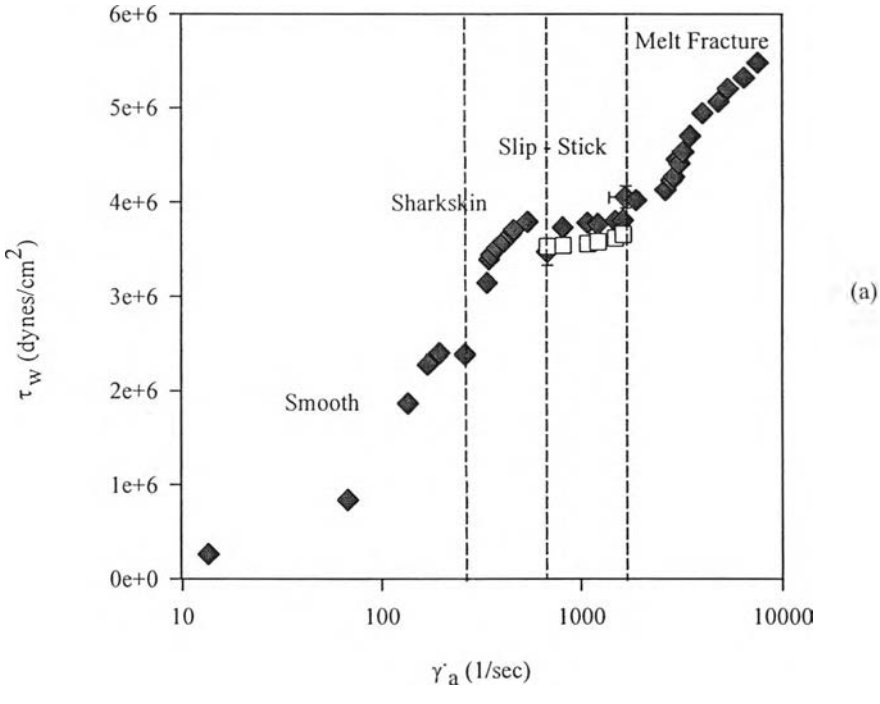

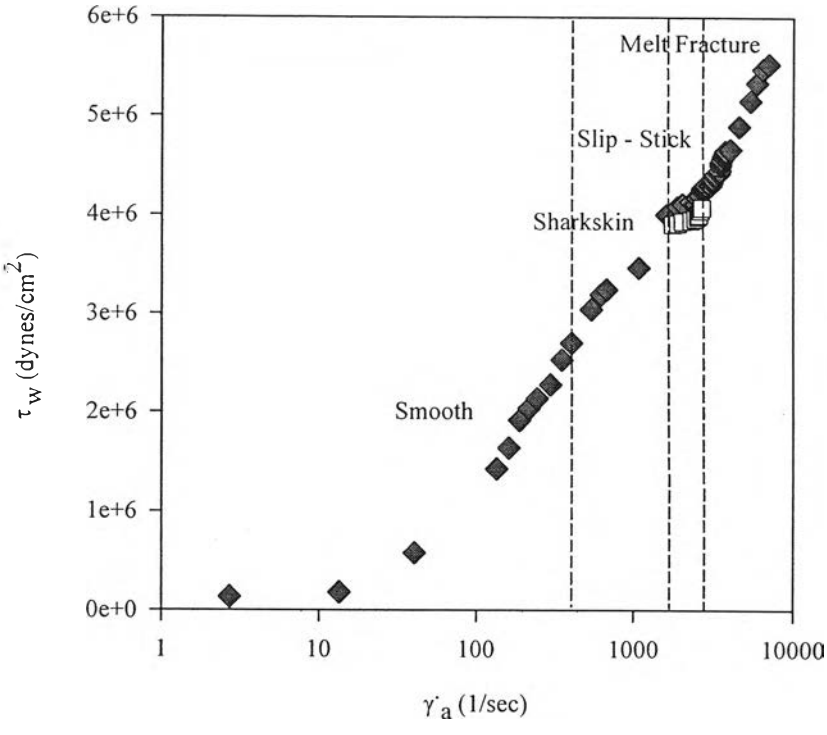
6e+6
5e+6
4e+6
3e+6
2e+6
1e+6
0e+0
1
10
100
1000
10000
Melt Fracture
Slip - Stick
Sharkskin
Smooth
τ_w (dynes/cm^2)
$\gamma^{\cdot}_a$ (1/sec)

(b)

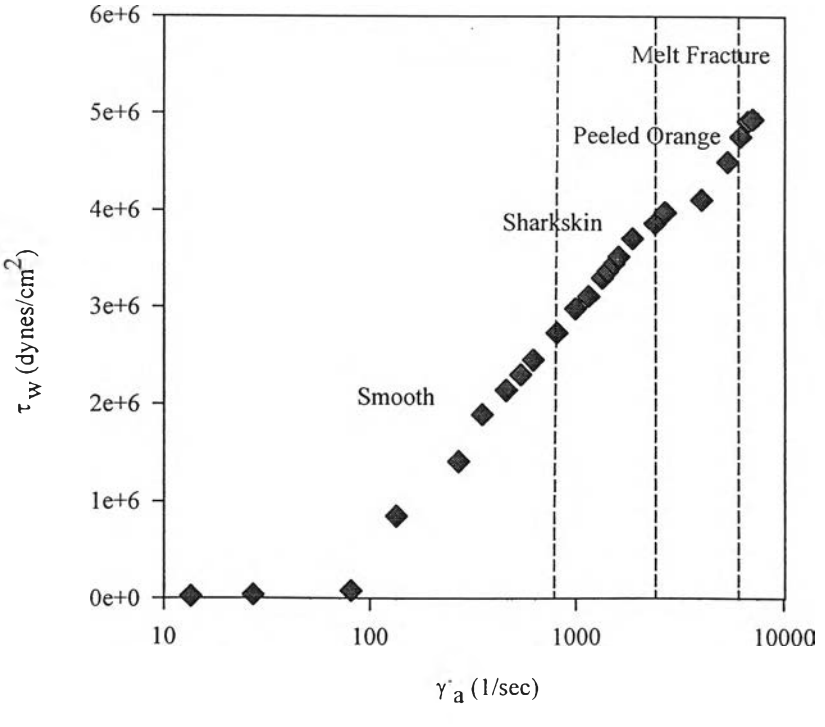
6e+6
5e+6
4e+6
3e+6
2e+6
1e+6
0e+0
10
100
1000
10000
Melt Fracture
Peeled Orange
Sharkskin
Smooth
τ_w (dynes/cm^2)
$\gamma^{\cdot}_a$ (1/sec)

(c)

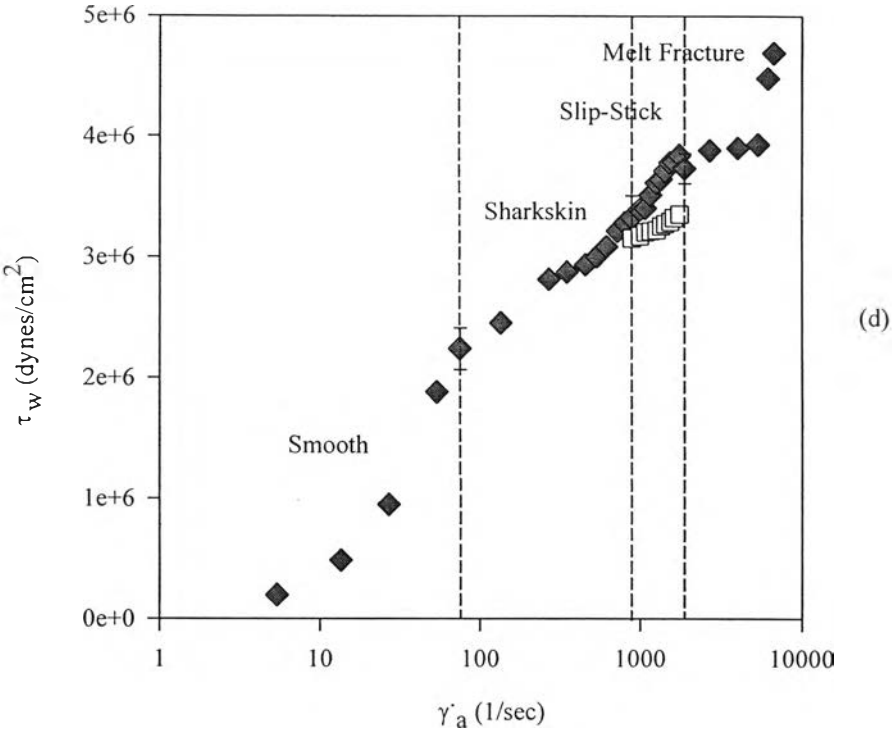
5e+6
4e+6
3e+6
2e+6
1e+6
0e+0
1
10
100
1000
10000
Melt Fracture
Slip-Stick
Sharkskin
Smooth
τ_w (dynes/cm^2)
$\gamma^{\cdot}_a$ (1/sec)

(d)

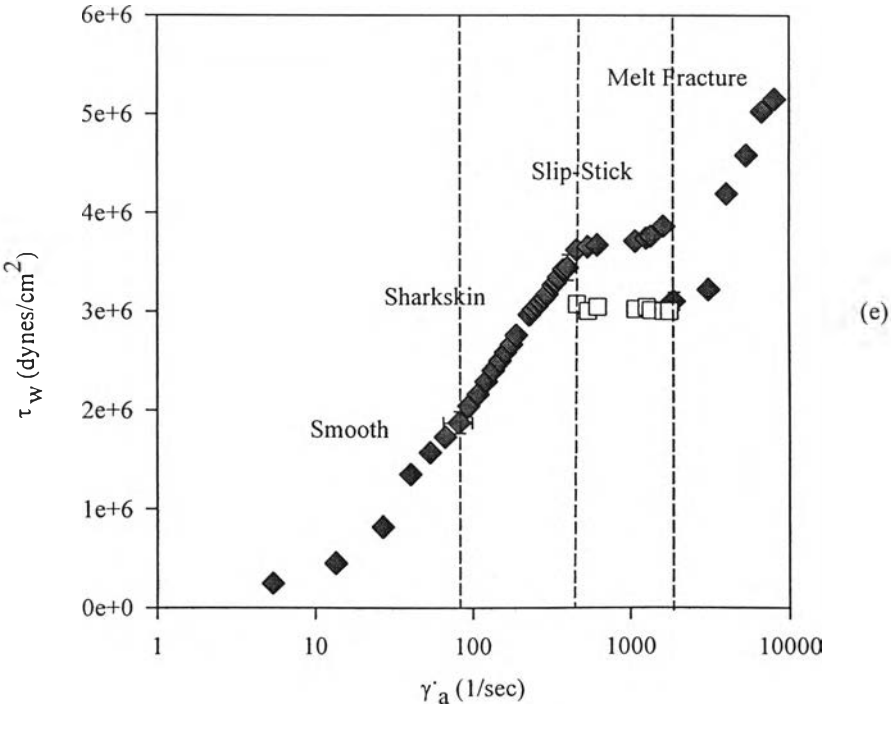
6e+6
5e+6
4e+6
3e+6
2e+6
1e+6
0e+0
1
10
100
1000
10000
Melt Fracture
Slip-Stick
Sharkskin
Smooth
τ_w (dynes/cm^2)
$\gamma^{\cdot}_a$ (1/sec)

(e)

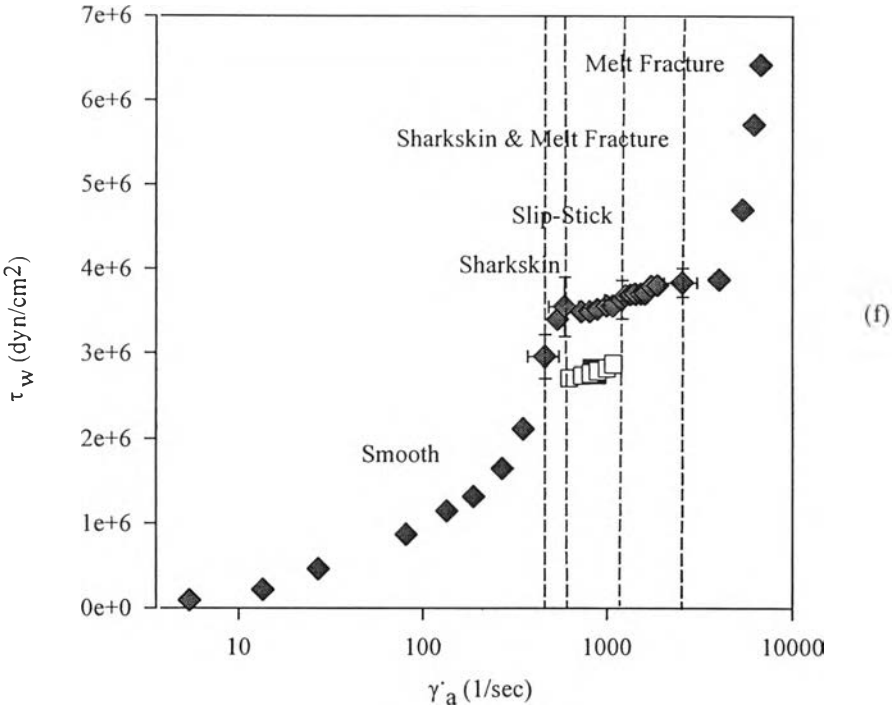

Figure 3.1 Flow curves at 190 ^{o}C: a) LLDPE (L2009F); b) LLDPE (L2020F); c) MDPE (M3204RU); d) HDPE (N3260); e) HDPE (H5690S); f) HDPE (R1760).

3.1.2 Surface Textures of L2009F

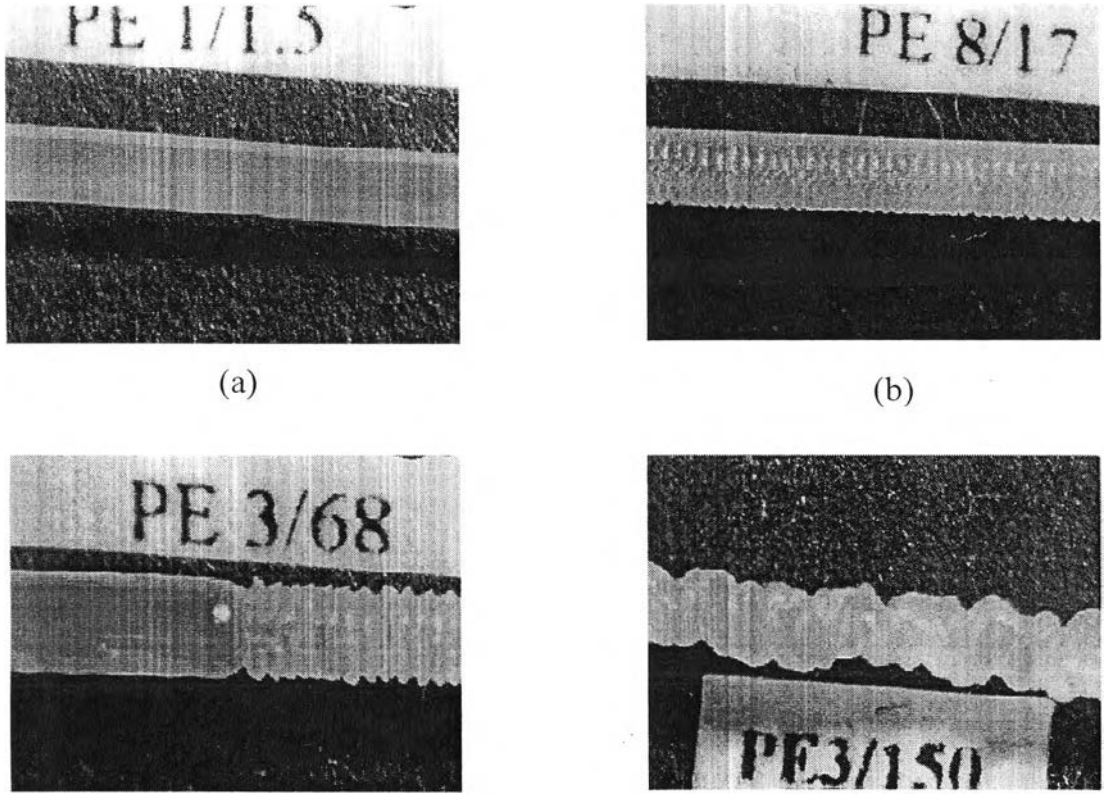

(a) (b)

(c) (d)

Figure 3.2 Skin textures of L2009F at 190 °C: a) smooth; b) sharkskin; c) slip - stick; d) melt fracture.

LLDPE, MDPE and HDPE of different molecular weights produce a similar skin defect in each regime. The photographs of skin defects are shown in Figures 3.2a-d for LLDPE (L2009F) melts at 190 °C.

Figure 3.2a shows a *smooth* skin extrudate of *Regime I*. At 20× magnification, we notice that the skin texture is apparently smooth.

Figure 3.2b shows a *sharkskin* extrudate of *Regime II*. It has a similar appearance to those sharkskins found in the previously published literature (*Kalika and Denn, 1987*).

Figure 3.2c shows an alternating sharkskin/smooth extrudate. The smooth segment is the same as the extrudate found in *Regime I*. The sharkskin segment is the same as the extrudate found in *Regime II*. Our identification of the skin defect is the same as other previous investigators who sometimes employed the name *slip-stick* (*Kalika and Denn, 1987*).

Figure 3.2d shows *a melt fracture* extrudate in *Regime IV*. We notice here that the surface distortions are very severe. The magnitude of random variations in the extrudate cross section is comparable to the capillary diameter. Our identification of the skin defect is the same as other previous investigators who sometimes employed the name *wavy fracture*. Wavy fracture is the most form of extrudates distortion with the distortion depth on the order of the extrudate diameter (*Kalika and Denn, 1987*).

3.1.3 Critical Values

The conditions for the onset of various regimes for our samples of different molecular weights are summarized in Table 3.2 below.

Table 3.2 The critical wall shear stress ($\tau_{w,c}$) and strain rates ($\dot{\gamma}_a$) of LLDPE, MDPE and HDPE's at the onsets of flow regimes

Table 3.2 The critical wall shear stress ($\tau_{w,c}$) and strain rates (γ_a) of LLDPE, MDPE and HDPE's at the onsets of flow regimes

Regime	Critical Data	L2009F	L2020F	M3204RU	N3260	H5690S	R1760
II	γ_a (1/sec)	265	325	730	75	83	461
sharkskin	$\tau_{w,c}$ (dynes/cm^2)	2.38×10^6	2.61×10^6	2.83×10^6	2.24×10^6	2.28×10^6	2.46×10^6
III	γ_a (1/sec)	677	1760	2430	388	459	591
slip-stick	$\tau_{w,c}$ (dynes/cm^2)	3.47×10^6	3.94×10^6	3.78×10^6	3.32×10^6	3.51×10^6	3.55×10^6
IV	g_a (1/sec)	3020	3520	7040	1087	1110	1215
melt	$t_{w,c}$ (dynes/cm^2)	4.45×10^6	4.54×10^6	4.94×10^6	3.73×10^6	3.75×10^6	3.83×10^6
fracture							

It can be seen from Table 3.2 that the critical wall shear stress is independent of molecular weight. The critical wall shear stress of sharkskin increases from 2.24×10^6 dynes/cm^2 to 2.46×10^6 dynes/cm^2 when the molecular weight changes from 1.92×10^4 g/mol to 1.36×10^4 g/mol for HDPE and 2.38×10^6 dynes/cm^2 to 2.83×10^6 dynes/cm^2 [nearly the same as (Kalika and Denn, 1987) varies from 2.57×10^6 dynes/cm^2 to 4.10×10^6 dynes/cm^2] when the molecular weight changes from 1.03×10^5 g/mol to 3.36×10^4 g/mol for LLDPE and MDPE. The range of the critical wall shear stress for HDPE is slightly greater than that of LLDPE and MDPE. The critical wall shear stress depends on the regime or the skin texture that appear. The critical strain rate is higher for a HDPE or a LLDPE melt with a lower molecular weight. This is simply because HDPE, LLDPE and MDPE with a lower molecular weight has a lower viscosity, therefore the critical strain rate has to be higher if the critical wall stress is to be the same. Thus, one expects the critical value of shear strain rate to decrease as the molecular weight increases (*Spencer and Dillon 1949, Brydson 1970, and Vlachopoulos and Glyde 1971*). This present results show this behavior , as shown in Table 3.2. For some polymers, at least, the critical shear stress $\tau_{w,c}$ is inversely proportional to the weight average molecular weight (*Spencer and Dillon 1949*).

Table 3.3 The critical wall shear stress ($\tau_{w,c}$) and strain rates ($\dot{\gamma}_a$) of HDPE (H5690S) and LLDPE (L2020F) at the onset of sharkskin regimes function of melt temperature

Materials	Regime	Critical Data	210 °C	200 °C	190 °C	180 °C	170 °C	160 °C	150 °C
H5690S	II	$\dot{\gamma}_a$ (1/sec)	135	137	138	144	157	221	229
	sharkskin	$\tau_{w,c}$ (dynes/cm^2)	2.22×10^6	2.24×10^6	2.26×10^6	2.28×10^6	2.29×10^6	2.30×10^6	2.31×10^6
L2020F	II	$\dot{\gamma}_a$ (1/sec)	-	317	325	460	541	623	-
	sharkskin	$\tau_{w,c}$ (dynes/cm^2)	-	2.59×10^6	2.61×10^6	2.92×10^6	3.26×10^6	3.72×10^6	-

Table 3.3 shows the critical wall shear stress ($\tau_{w,c}$) and strain rates ($\dot{\gamma}_a$) of HDPE (H5690S) and LLDPE (L2020F) at the onset of sharkskin regimes as functions of the melt temperature. The critical wall shear stress decreases from 2.31×10^6 dynes/cm^2 to 2.22×10^6 dynes/cm^2 when the melt temperature is raised from 150 °C to 210 °C for HDPE (H5690S) and it decreases from 3.72×10^6 dynes/cm^2 to 2.59×10^6 dynes/cm^2 when the melt temperature is raised from 160 °C to 200 °C for LLDPE (L2020F). Therefore, the onset of the sharkskin extrudates does depend on temperature. As the melt temperature is raised, chain disentanglements become dynamically simpler; consequently the force required must be reduced. Increasing temperature raises shear strain rate consistent with published data that higher temperatures require higher rates of shear in order to reach a critical fracture stress (*Howells and Benbow, 1962*).

Table 3.4 The critical wall shear stress ($\tau_{W,C}$) and strain rates ($\gamma \cdot_a$) of HDPE (H5690S) and LLDPE (L2020F) at the onset of sharkskin regimes function of die geometry

Materials	Regime	Critical Data	l_c/d_c = 7.01 l_C = 13.775 d_C =1.9675	l_c/d_c = 33.4 l_C = 25.105 d_C = 0.7525	l_c/d_c =40.1 l_C = 50.188 d_C = 1.2550
H5690S	II sharkskin	γ_a (1/sec) $\tau_{w,c}$ (dynes/cm^2)	70 2.38×10^6	83 2.65×10^6	112 2.77×10^6
L2020F	II sharkskin	γ_a (1/sec) $\tau_{w,c}$ (dynes/cm^2)	310 2.61×10^6	325 2.78×10^6	342 2.98×10^6

Table 3.4 shows the critical wall shear stress ($\tau_{W,C}$) and strain rate ($\gamma \cdot_a$) of HDPE (H5690S) and LLDPE (L2020F) at the onset of sharkskin regimes as functions of die geometry. Here the HDPE (H5690S) and LLDPE (L2020F) melt temperature was fixed at 190 ^oC. The critical wall shear stress increases from 2.38×10^6 dynes/cm^2 to 2.77×10^6 dynes/cm^2 for HDPE (H5690S) and 2.61×10^6 dynes/cm^2 to 2.98×10^6 dynes/cm^2 for LLDPE (L2020F) when the die geometric factor l_C/d_C increases from 7.00 to 40.14. The dependence of the critical wall shear stress on l_C/d_C ratio can be explained as follows. For a longer die the necessary pressure upstream required to extrude the melt is expectedly higher; therefore a larger melt density and a smaller free volume fraction are to be expected. A melt with a smaller free volume would require a larger force to create a thin disentanglement layer and correspondingly a larger critical wall shear stress. For short l_C/d_C , the stress does not have time to relax prior to exiting the die and as a result the onset of surface fracture is observed at lower values of the wall shear stress than in longer l_C/d_C dies (*Moynihan, Baird and Ramanathan, 1990*). The slight increase

of the critical wall shear stress with the l_c/d_c ratio is consistent with previous published data (*Ramamurthy 1986 and Kalika and Denn, 1987*).

3.2 Rheological Characterizations

Rheological properties of polymer melt are usually highly temperature dependent. This means that to obtain a complete picture of the behavior, even if the behavior is linear, experiments must be carried out at several temperatures. It is often found that data, for example G′(w) and G″(w), taken at several temperatures can be brought together on a single master curve by the mean of "time-temperature superposition" (*Ferry, 1981*). This greatly simplifies the description of the effect of temperature. Futhermore, it is possible the display on a single curve the material behavior covering a much broader range of time or frequency than can ever be measured at a single temperature. Materials whose behavior can be displayed in this way are said to be "thermorheologically simple" (*Dealy Wissbrun, 1989*).

The behavior of polymer melts, can be divided into the glassy, transition, plateau and terminal zones. At very short times the response is glassy. The modulus is large (typically 10^{11} dynes/cm^2). It falls rapidly as the chains relax locally, and then over progressively longer chain distances. For short chains the relaxation proceeds smoothly to zero. For long chains the relaxation rate slows, and the modulus remains relatively flat for a time before finally resuming its rapid relaxation to zero. This *intermediate zone* separates the short time response the transition zone, where the chain architecture has little effect, from the long time response where such architectural features as molecular weight, molecular weight distribution, and long-chain branching have a profound effect. The response at intermediate times resembles that of a network. The width of the plateau increases rapidly with chain length, but the plateau modulus G^0_N is independent of chain length.

3.2.1 G′ vs. ω and G″ vs. ω

We can construct a plot between G′ vs. ω and G″ vs. ω obtained from parallel plates rheometer at the different temperatures. The data of LLDPE (L2009F) are shown in Figures 3.4a and Figures 3.4b below and graphs of other materials are shows in the appendix. Our experiment used spacing gap about 0.599 mm. First measurement was Dynamic Strain Sweep Default Test. We can selected *DStmSwp* from the Description of test Parameters. The sweep mode was log. The strain was varied between 0.1-100 rad/sec. In our experiment, we used the percentage of strain ofabout 4 and the frequency 1 rad/sec, temperature 190 °C, and selected 5 point per decade. The next measurement mode was Dynamic Frequency/Temperature Sweep. We can selected *DF/T Swp* from the Description of test Parameters. The sweep mode was log. The frequency was from 0.1-100 rad/s The temperature was varied between 230-110 °C, and temperature increment was 10 °C for the ranges 230-120 °C and 2 °C for the ranges 118-110 °C. Soak time was 180 seconds.

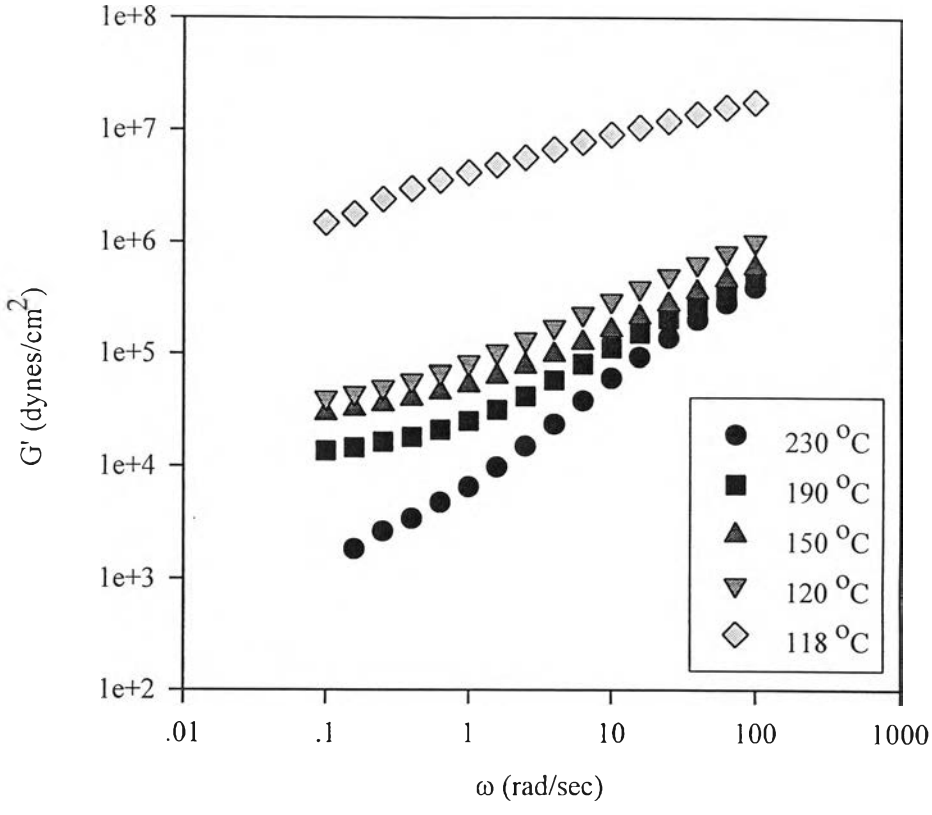

(a)

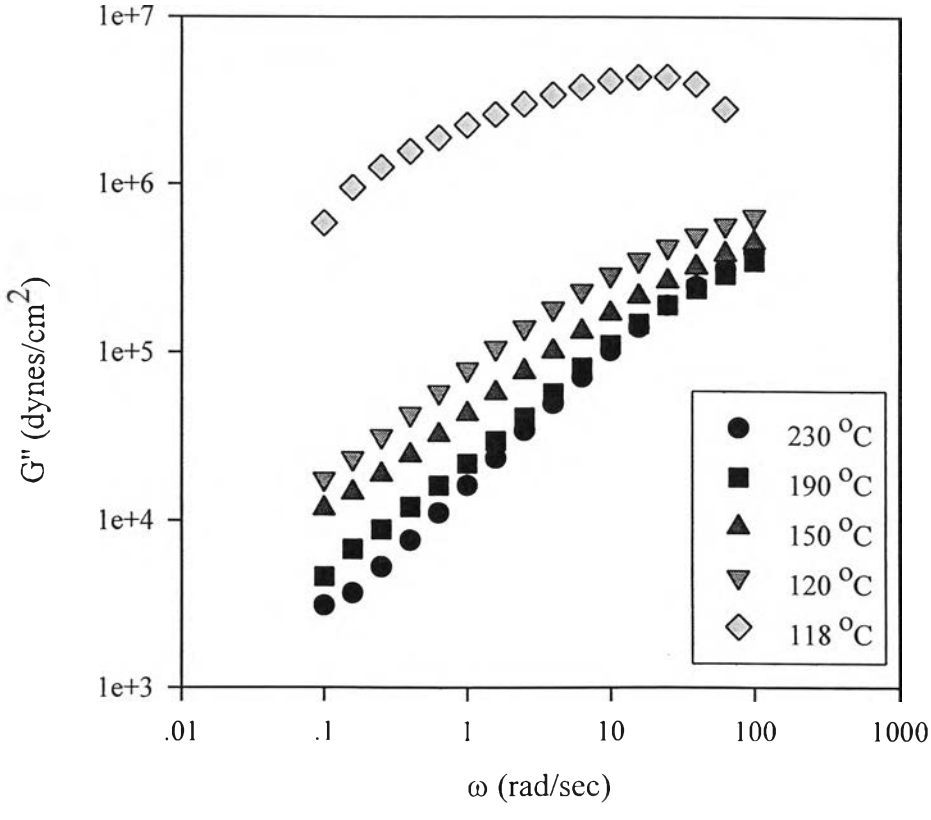

(b)

Figure 3.3 G vs. ω of LLDPE (L2009F) at 190 °C: a) G′ vs. ω; b) G″ vs. ω.

3.2.2 Master Curves of HDPE ,LLDPE and MDPE

The Master Curve can be obtained through measurement of G′ as a function of frequency at various temperatures. G′ curves at different temperatures were shifted horizontally and vertically to form a single master curve at a fixed reference temperature which is the same as on of the melt flow temperature (*Rheo. Sci, 1995*). The vertical shift factor used was calculated from $b_T = T_0/T$, whereas the horizontal shift factor a_T was determined emperically.

Determination of G_N^o value of each material can be identified as the value of G′ in a zone where G″ has a peak and then falls below the storage modulus over the entire plateau zone. This decrease in G″ below G′ only occurs in entangled melts and refects the dominance of elasticity and the relatively small viscous energy discipation in the rubbery zone (*Dealy and Wissbrun, 1989*). A another method is to choose the value of the modulus at the inflection point of G′ (*Graessley, 1974*).

In our work, we determined the apparent G′ from plateau zones for two LLDPEs (L2009F, L2020F). For other materials where the plateau could not be obtained directly, we used *the fit equation* to determine the G_N^o values for MDPE (M3204RU) and HDPE (N3260, H5690S, R1760). The equation we used to evaluate G_N^o was $b_T G'(\omega) = G_N^o + C_1(a_T\omega)^{-C2}$,where C_1 and C_2 are constants. For the procedure, we plotted a graph between log (G_N^o -b_TG′ (ω)) versus log $a_T\omega$. For each material, we selected G_N^o that maximized r^2 (the fitting coefficient) where C_1 was the intercept and C_2 was the slope.

Master curves of all materials are shown below in Figure 3.4a - Figure 3.4f.

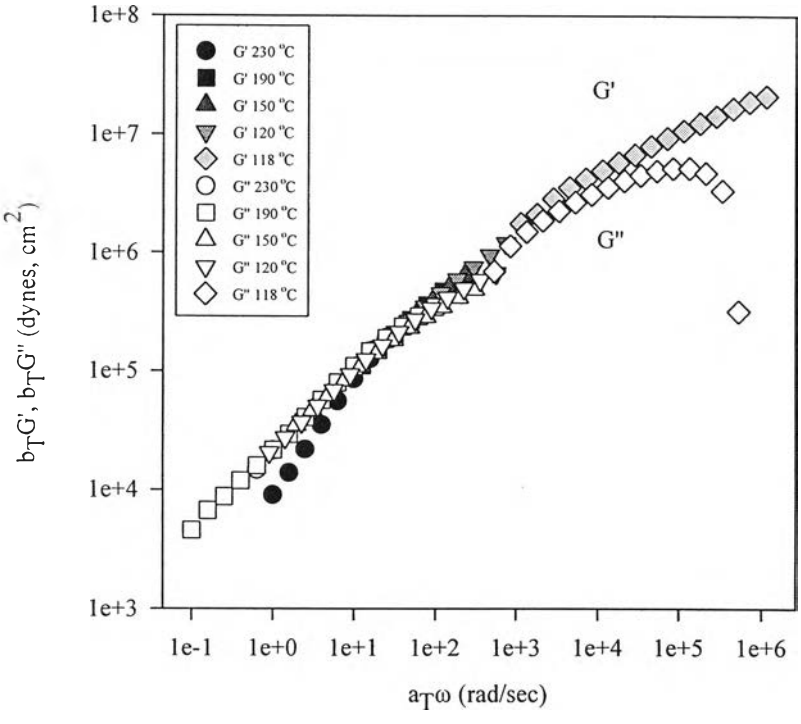
1e+8
1e+7
1e+6
1e+5
1e+4
1e+3
1e-1
1e+0
1e+1
1e+2
1e+3
1e+4
1e+5
1e+6
$b_T G'$, $b_T G''$ (dynes, cm^2)
$a_T \omega$ (rad/sec)
G' 230 °C
G' 190 °C
G' 150 °C
G' 120 °C
G' 118 °C
G" 230 °C
G" 190 °C
G" 150 °C
G" 120 °C
G" 118 °C
G'
G"

(a)

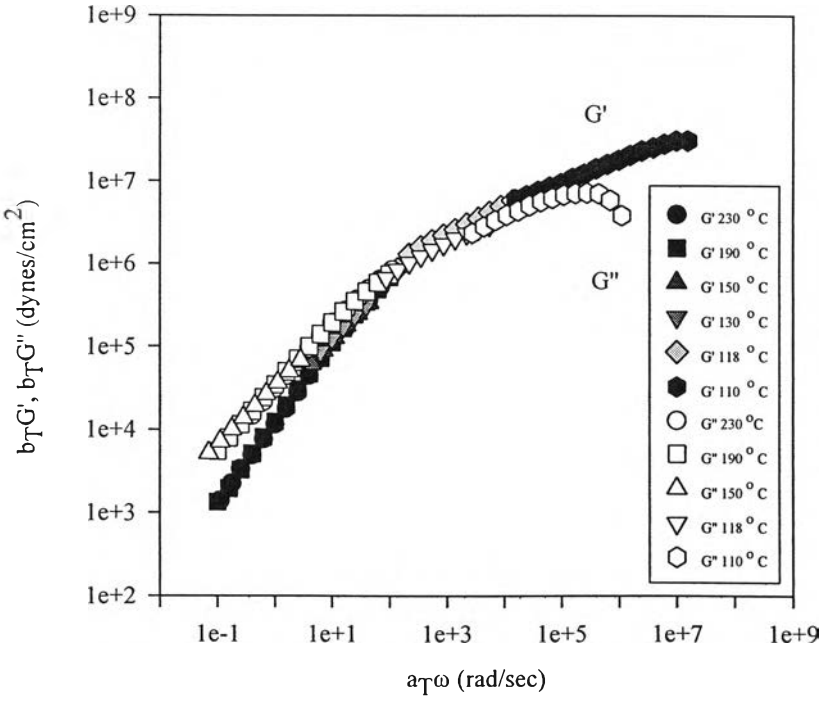
1e+9
1e+8
1e+7
1e+6
1e+5
1e+4
1e+3
1e+2
1e-1
1e+1
1e+3
1e+5
1e+7
1e+9
$b_T G'$, $b_T G''$ (dynes/cm^2)
$a_T \omega$ (rad/sec)
G' 230 °C
G' 190 °C
G' 150 °C
G' 130 °C
G' 118 °C
G' 110 °C
G" 230 °C
G" 190 °C
G" 150 °C
G" 118 °C
G" 110 °C
G'
G"

(b)

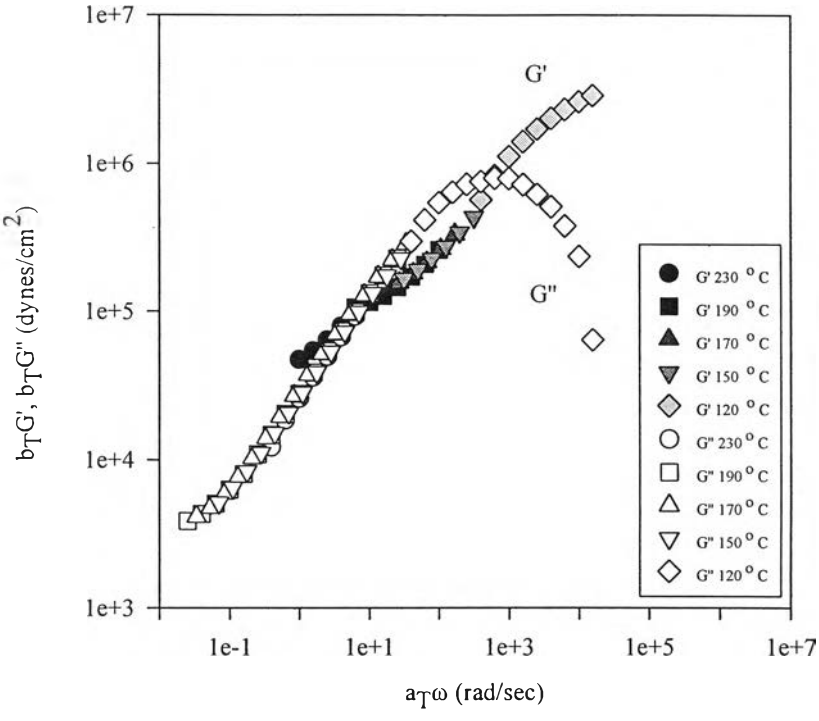
1e+7
1e+6
1e+5
1e+4
1e+3
G'
G"
G' 230 °C
G' 190 °C
G' 170 °C
G' 150 °C
G' 120 °C
G" 230 °C
G" 190 °C
G" 170 °C
G" 150 °C
G" 120 °C
1e-1
1e+1
1e+3
1e+5
1e+7
$b_T G'$, $b_T G''$ (dynes/cm^2)
$a_T \omega$ (rad/sec)

(c)

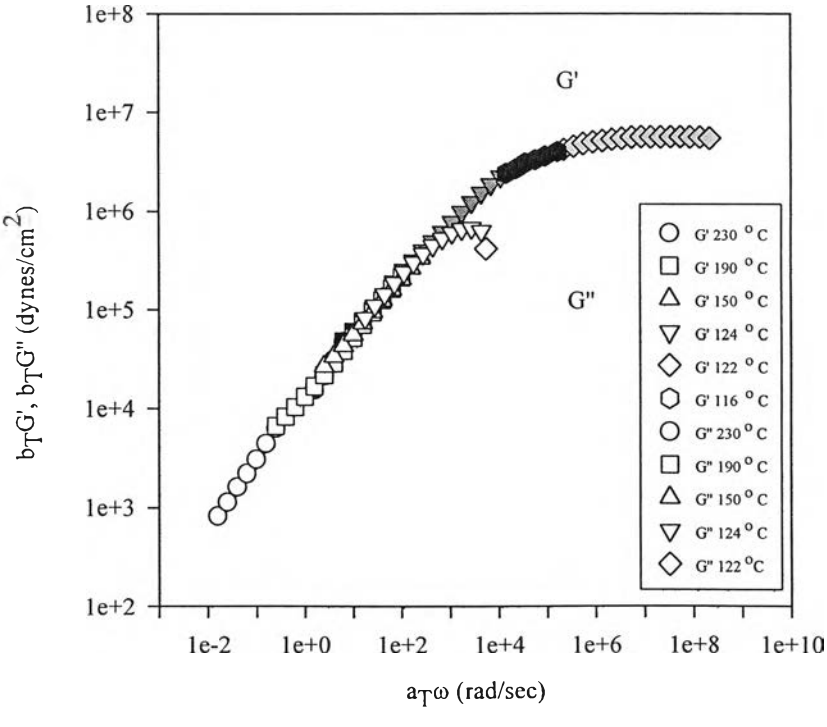
1e+8
1e+7
1e+6
1e+5
1e+4
1e+3
1e+2
G'
G"
G' 230 °C
G' 190 °C
G' 150 °C
G' 124 °C
G' 122 °C
G' 116 °C
G" 230 °C
G" 190 °C
G" 150 °C
G" 124 °C
G" 122 °C
1e-2
1e+0
1e+2
1e+4
1e+6
1e+8
1e+10
$b_T G'$, $b_T G''$ (dynes/cm^2)
$a_T \omega$ (rad/sec)

(d)

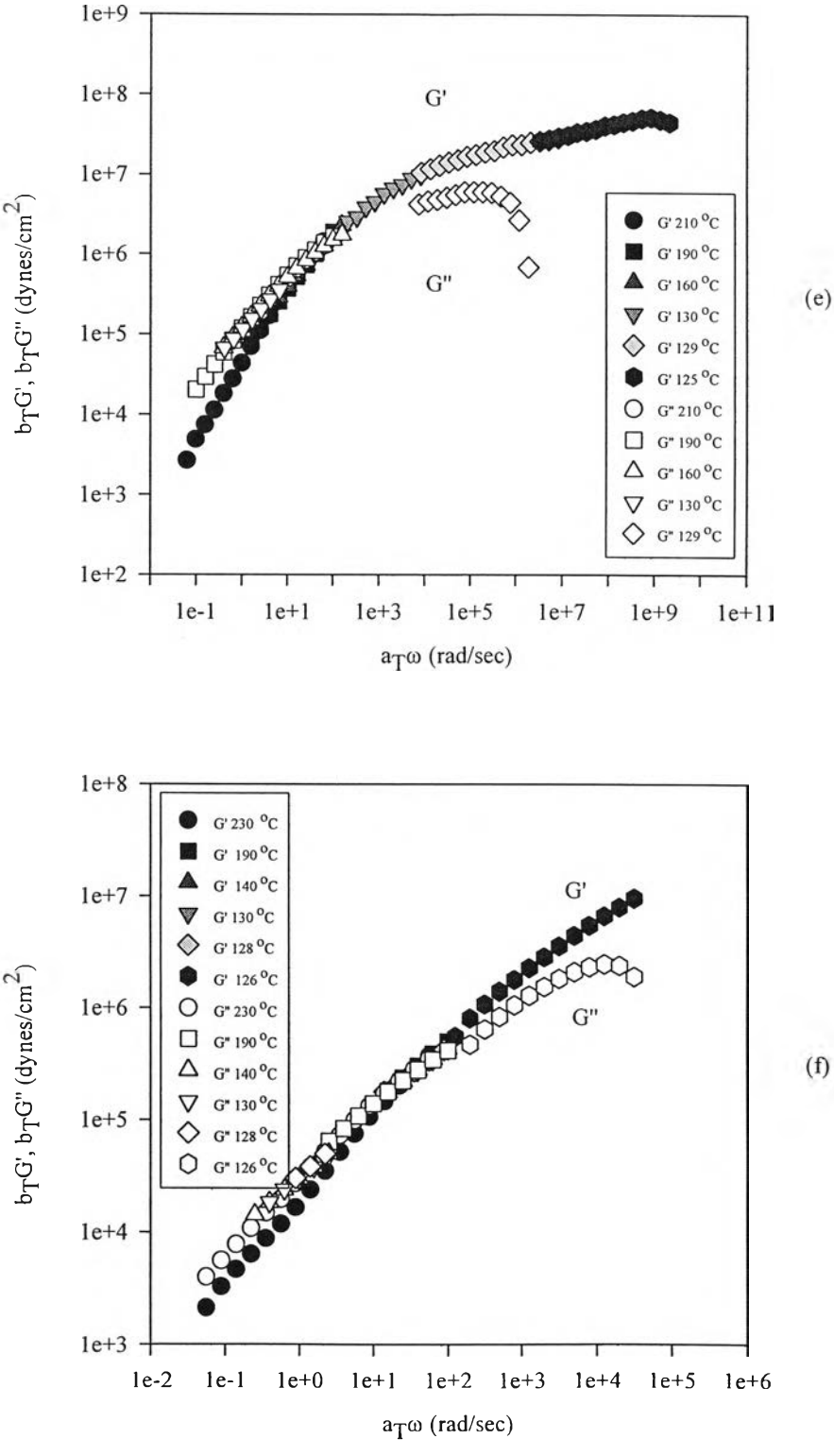

Figure 3.4 Master curves at 190 °C: a) LLDPE (L2009F); b) LLDPE (L2020F); c) MDPE (M3204RU); d) HDPE (N3260); e) HDPE (H5690S); f) HDPE (R1760).

Table 3.5 G_N^o of LLDPE, MDPE and HDPE melts at 190 °C

PE	Materials	$M_w \times 10^{-4}$ (g/mol)	$\eta_0 \times 10^{-4}$ (P)	$\eta_0^* \times 10^{-5}$ (P)	$G_N^o \times 10^{-7}$ (dynes/cm^2)
LLDPE	L2009F	10.3	5.0	10	3.0
LLDPE	L2020F	6.07	3.8	5.2	3.3
MDPE	M3204RU	3.36	*	*	3.3
HDPE	N3260	1.92	*	*	1.7
HDPE	H5690S	1.84	20	25	1.8
HDPE	R1760	1.36	*	*	1.7

* Cannot be determined accurately from extrabolation.

Table 3.5 shows G_N^o values of LLDPE, MDPE and HDPE melts at 190 °C. The measured G_N^o values are found to be between 1.7×10^7 dynes/cm^2 - 3.3×10^7 dynes/cm^2, independent of molecular weight and consistent with a quoted literature value (*Ferry, 1981*) of $G_N^o = 2.29\times10^6$ dynes/cm^2 of polyethylene.

Table 3.6 G_N^o of LLDPE (L2020F) and HDPE (H5690S) melts as functions of the melt temperature

Temperature (°C)	210	200	190	180	170	160	150
HDPE *(H5690S)* $G_N^o \times 10^{-7}$ (dynes/cm^2)	3.44	3.37	3.30	3.23	3.16	3.09	3.01
$\eta_0' \times 10^{-5}$ (P)	1.2	1.6	2.0	2.5	4.7	5.2	6.2
$\eta_0^* \times 10^{-6}$ (P)	1.3	1.6	2.5	4.0	5.7	8.0	8.5
LLDPE *(L2020F)* $G_N^o \times 10^{-7}$ (dynes/cm^2)	-	2.09	1.80	1.76	1.72	1.69	-
$\eta_0' \times 10^{-4}$ (P)	-	*	3.8	6.0	7.0	7.3	-
$\eta_0^* \times 10^{-5}$ (P)	-	5.0	5.2	6.5	7.0	*	-

* Cannot be determined accurately from extrabolation..

Table 3.6 shows G_N^o values of LLDPE (L2020F) and HDPE (H5690S) melts as functions of the melt temperature. G_N^o values vary from 3.01 $\times 10^7$ dynes/cm^2 to 3.44$\times 10^7$ dynes/cm^2 in the range of melt temperature from 150 °C to 210 °C for HDPE (H5690S) melts and 1.69$\times 10^7$ dynes/cm^2 to 2.09$\times$ 10^7 dynes/cm^2 in the range of melt temperature from 160 °C to 200 °C for LLDPE (L2020F) melts. We can conclude that G_N^o values vary slightly with temperature. The entanglement storage modulus, G_N^o, as determined from the

parallel plate rheometer is simply a constant consistent with *Mark, Eisenberg, Graessley, Mandelkern and Koening, 1984* data where G''_N is practically independent of temperature because temperature shifts the viscoelastic functions along the modulus and time (or frequency) scales without changing their shapes. In fact, the modulus shift is extremely weak. The major effect of temperature change is simply to rescale the time. Raising the temperature shifts the response curves to smaller times (higher frequencies). At the molecular level, the rate of Brownian motion is increased but the molecular oganization and the structure is practically unchanged. Measurements at different temperatures can thus be reassembled to form a master curve, covering may more decades than is possible by measurements at any single temperature.

3.2.3 Cox-Merz Rule of HDPE (H5690S) and LLDPE (L2020F)

Cox-Merz (1985) equated the complex viscosity (η^*) vs. frequency (ω) obtained from a parallel plates rheometer with the steady state viscosity (η) vs. apparent strain rate ($\dot{\gamma}_a$) obtained from a capillary rheometer. Figures 3.5a and b are plots of η vs. $\dot{\gamma}_a$ and η^* vs. ω for HDPE (H5690S) and LLDPE (L2020F) melts respectively at 190 ^oC.

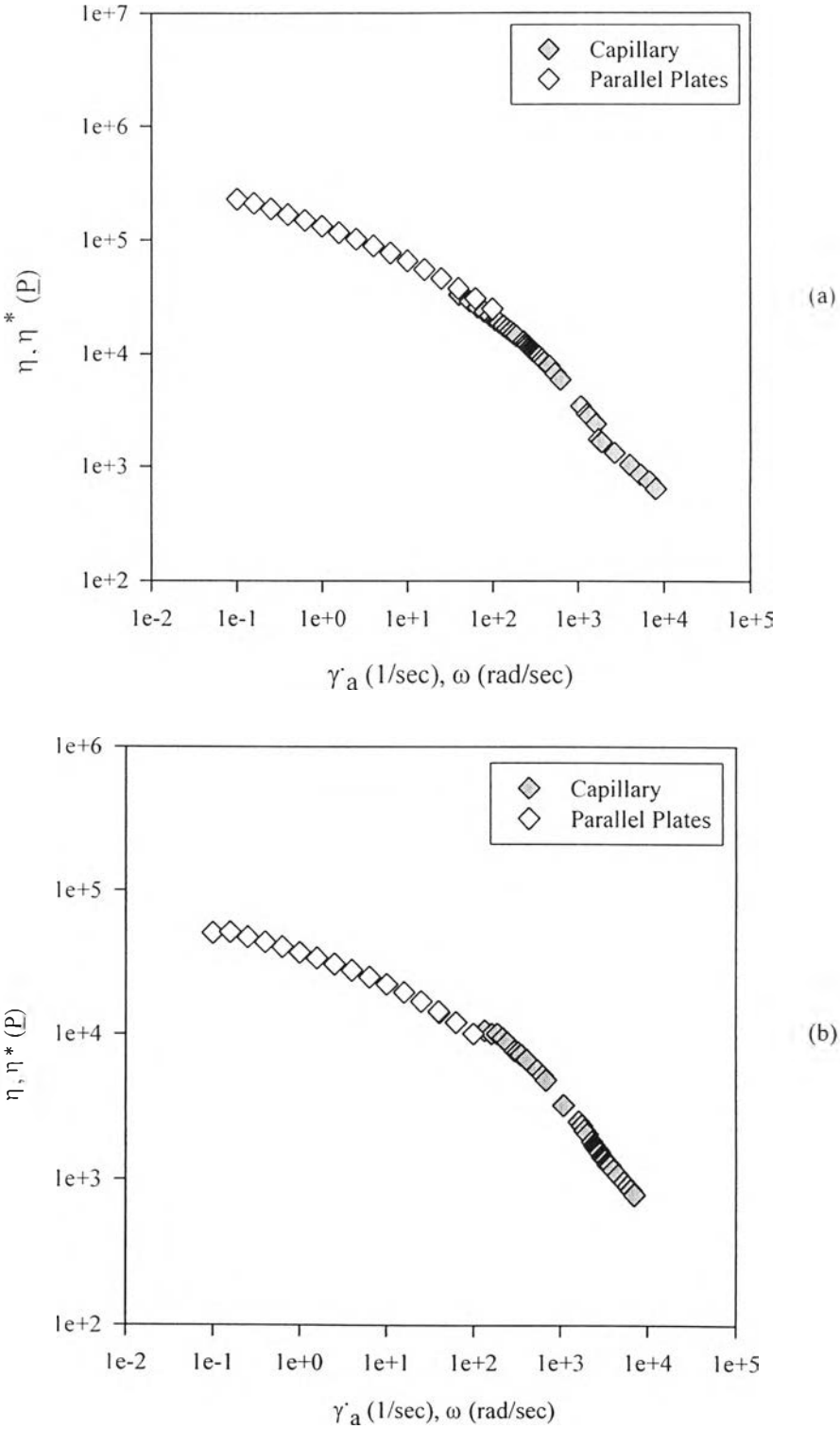

Figure 3.5 Cox-Merz rule at 190 ^{o}C: a) HDPE(H5690S); b) LLDPE(L2020F).

From Figures 3.5a and b, it can be seen that the partial collapse of the two viscometric functions, indicates that the Cox-Merz rule can be applied rather well to these two materials. The apparent success probably stems from the fact that l_c/d_c is above 30 and the entrance and exit losses can be neglected. The partial collapse between the apparent viscosity and the complex viscosity lends a support to the assumption that the apparent wall shear stress measured is approximately the same as the true wall shear stress.

For other materials (LLDPE; L2009F), (MDPE; M3204RU) and (HDPE; N3260, R1760), the Cox-Merz rule does not apply very well. Figures of the two viscometric functions of other materials can be seen in appendix. A very large change of viscosity over a narrow temperature range may indicate that a phase change has occured. An example of such a phase change is the melting of a few imperfect units on chains and it is difficult to detect crystallities, which act as crosslinks in the melts. Such a change in often accompanied by a drastic change in the shape of the flow curve. Other phase changes, such as a change from a miscible to immiscible mixture, will affect the flow curve similarly (*Ghijsels and Raadsen, 1980*). Another possible indication of such complexities is the failure of Cox-Merz rule as reparted by *Dealy and Wissbrun* : (*1989*).

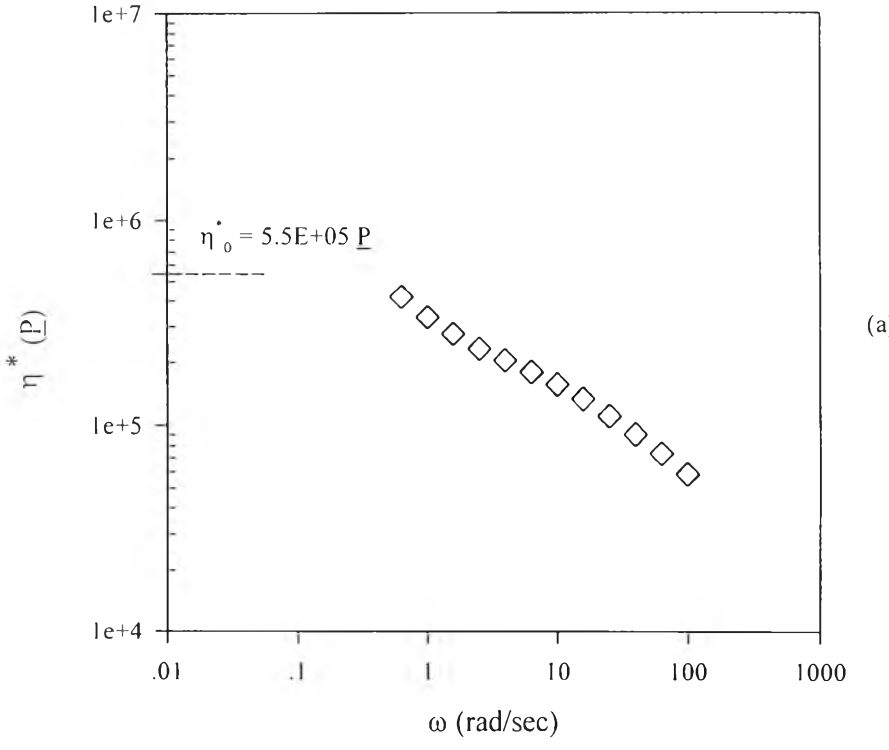

(a)

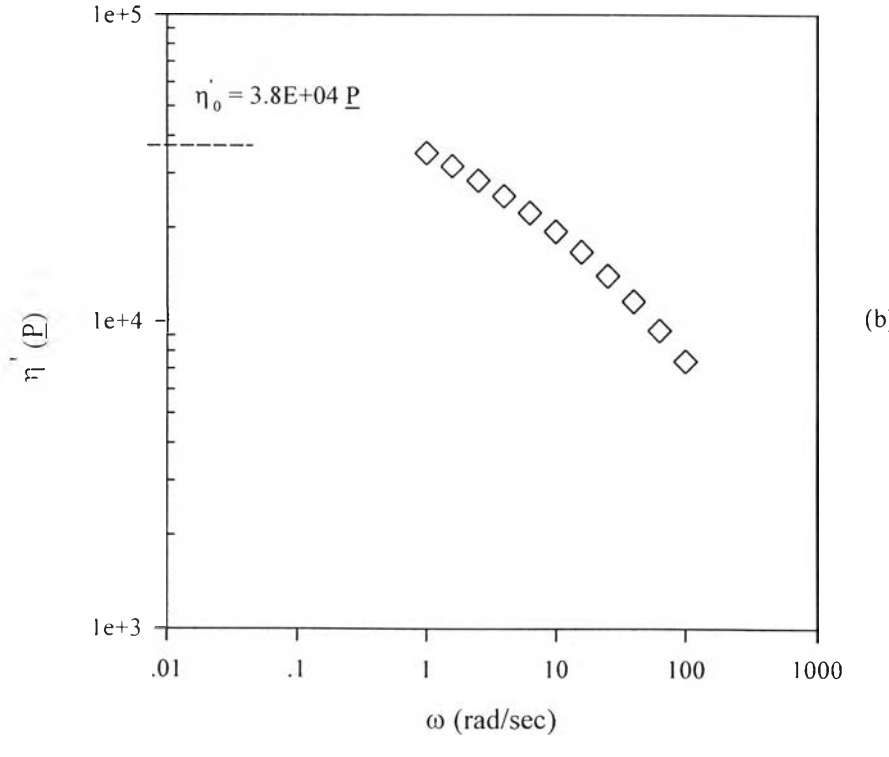

(b)

Figure 3.6 LLDPE (L2020F) at 190 °C: a) η_0^* vs. ω; b) η_0' vs. ω.

Figure 3.6 shows η_0^* vs. ω and η_0' vs. ω of LLDPE (L2020F) melt at 190 °C. From these graphs, we extrapolated the data to obtain the zero shear rate complex viscosity η_0^* and the zero shear rate loss viscosity η_0' at ω = 0.01 rad/sec. Table 3.5 shows that the zero shear rate complex viscosity η_0^* is 2.5×10^5 P and the zero shear rate loss viscosity η_0' is 2.0×10^5 P as the molecular weight is 1.84×10^4 g/mol for HDPE (H5690S) and η_0^* is 5.2×10^5 P to 1.0×10^6 P as η_0' increases from 3.8×10^4 P to 5.0×10^4 P as the molecular weight increases from 6.07×10^4 g/mol to 1.03×10^5 g/mol for LLDPE (L2009F, L2020F). For MDPE (M3204RU) and HDPE (N3260, R1760) melts we cannot determine the viscosities from extrabolation.

Table 3.6 shows η_0^* and η_0' of LLDPE (L2020F) and HDPE (H5690S) as functions of the melt temperature. The zero shear rate complex viscosity η_0^* of L2022F increases from 5.0×10^5 P to 7.0×10^5 P and the loss viscosity η_0' increases from 3.8×10^4 P to 7.3×10^4 P as the melt temperature decreases from 190 °C to 160 °C for LLDPE (L2020F) and η_0^* increases from 1.3×10^6 P to 8.5×10^6 P and η_0' increases from 1.2×10^5 P to 6.2×10^5 P as the temperature decreases from 210 °C to 150 °C for HDPE (H5690S).

In summary, the zero shear rate complex viscosity increases with polymer molecular weight and decreases as the melt temperature is raised; these results are consistent with published data (*Ferry, 1981*).

3.3 Effect of M_w on the sharkskin characteristic (λ_s,ε_s) of HDPE and LLDPE

3.3.1 Sharkskin Textures (λ_S,ε_S)

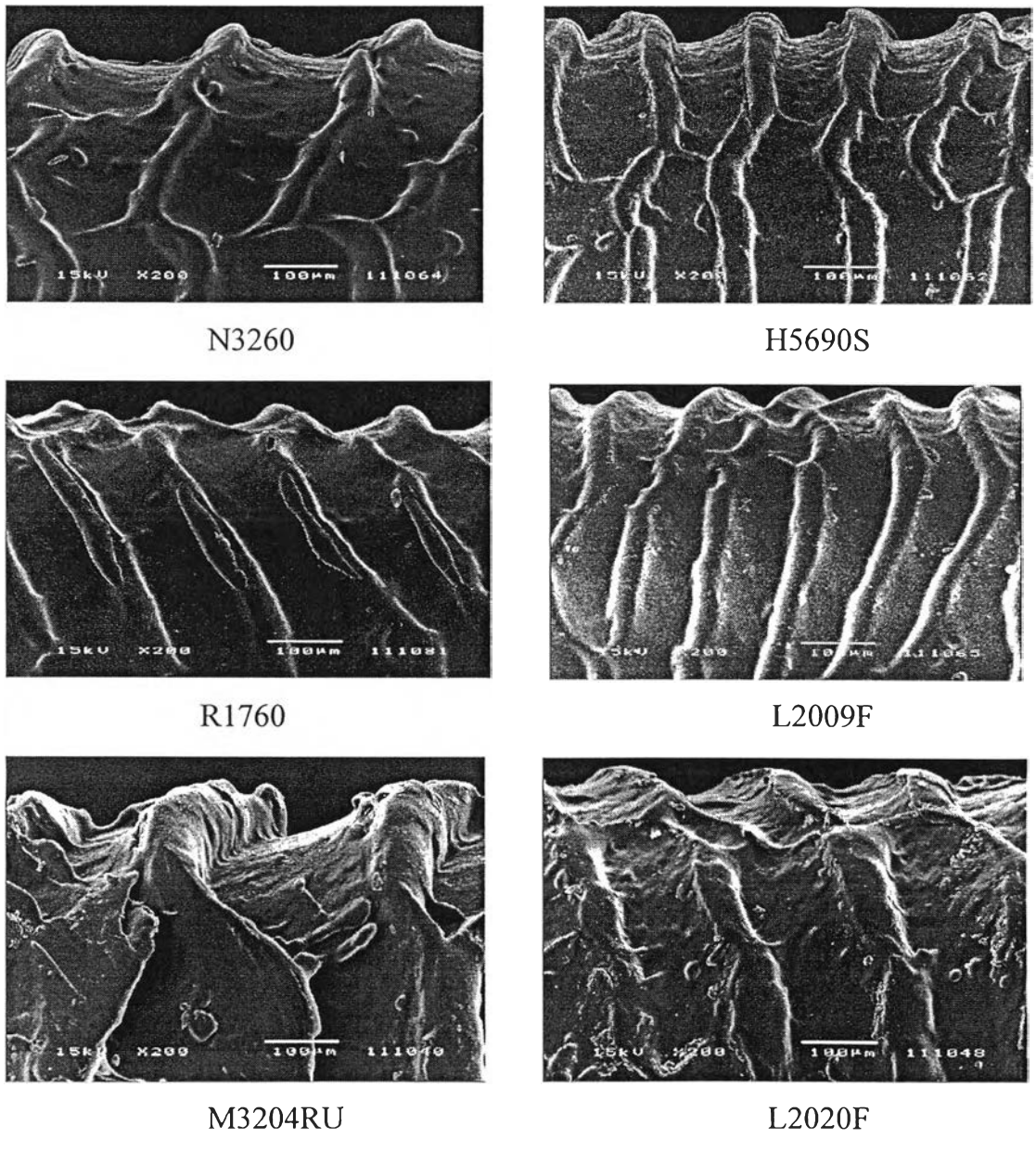

Figure 3.7 Sharkskin textures of HDPE (N3260, H5690S, R1760) and LLDPE (L2009F, L2020F), MDPE (M3204RU) at 190 ^{o}C.

Figure 3.7 shows sharkskin texture of HDPE (N3260, H5690S, R1760) and LLDPE (L2009F, L2020F), MDPE (M3204RU) at 190 ^{o}C. The characteristics of sharkskin (λ_S and ε_S) were determined from SEM (scanning electron microscope) micrographs. Figure 3.8 below shows how we measured the sharkskin wavelength (λ_S) and the sharkskin amplitude (ε_S). SEM digitized the pictures of the sharkskin defects by a ruler of *SemAfore* software program. The resolution of this ruler was 1/540 mm. We obtained the average value using at least three repeated measurements.

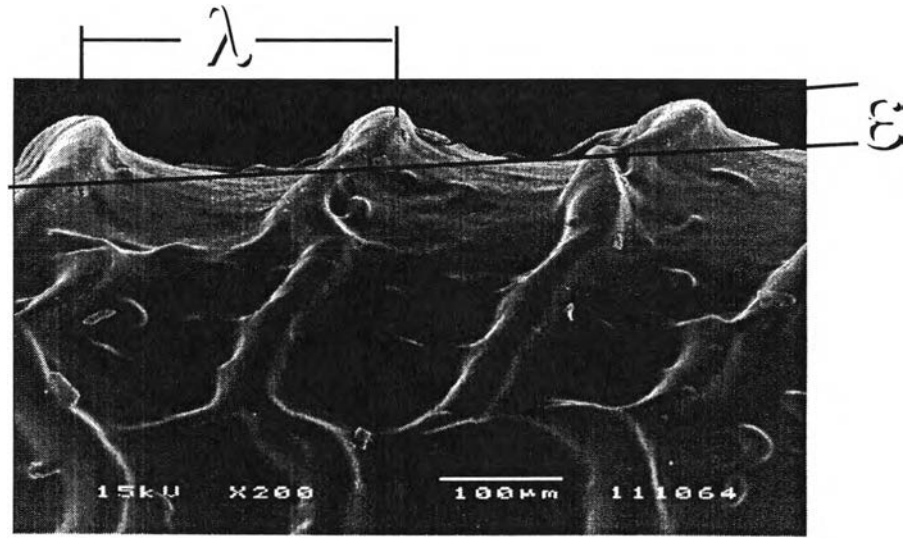

Figure 3.8 Sharkskin surface of HDPE (N3260) from SEM (200× magnification) and the measured wavelength (λ_S) and amplitude (ε_S) at 190 ^{o}C.

Table 3.7 Skin parameter and normalization of sharkskin defect of HDPE (N3260, H5690S and R1760) and LLDPE (L2009F, L2020F) and MDPE (M3204RU) at 190 ^{o}C, die no. 614

Materials	$M_W \times 10^{-4}$ (g/mol)	$\tau_{w,c} \times 10^{-6}$ (dynes/cm^2) (avg.)	$G_N^o \times 10^{-7}$ (dynes/cm^2)	S_R (avg.)	λ_S (avg.)	ε_S (avg.)	λ_S/ε_S (avg.)
R1760	1.36	2.26	3.0	0.074	208	43.7	4.76
H5690S	1.84	2.48	3.3	0.069	208	43.0	4.86
N3260	1.92	2.24	3.0	0.075	211	42.8	4.92
M3260RU	3.36	2.83	1.7	0.166	121	25.2	4.84
L2020F	6.07	2.61	1.8	0.145	129	26.1	4.92
L2009F	10.3	2.38	1.7	0.113	133	26.1	5.13

Table 3.7 shows sharkskin parameters and normalizations of sharkskin defect of HDPE (N3260, H5690S and R1760) and LLDPE (L2009F, L2020F) and MDPE (M3204RU) at 190 ^{o}C. We plotted graphs between λ_S vs. M_W and ε_S vs. M_W and λ_S/ε_S vs. M_W as shown in Figures 3.9a-c.

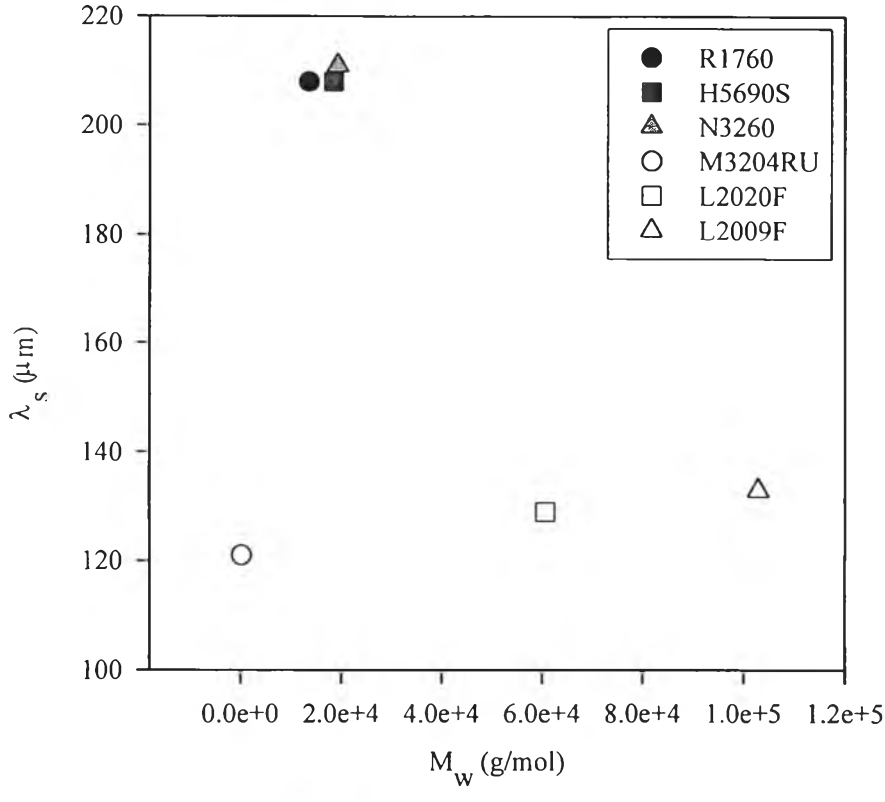
220
200
180
160
140
120
100
λ_s (μm)
R1760
H5690S
N3260
M3204RU
L2020F
L2009F
0.0e+0
2.0e+4
4.0e+4
6.0e+4
8.0e+4
1.0e+5
1.2e+5
M_w (g/mol)

(a)

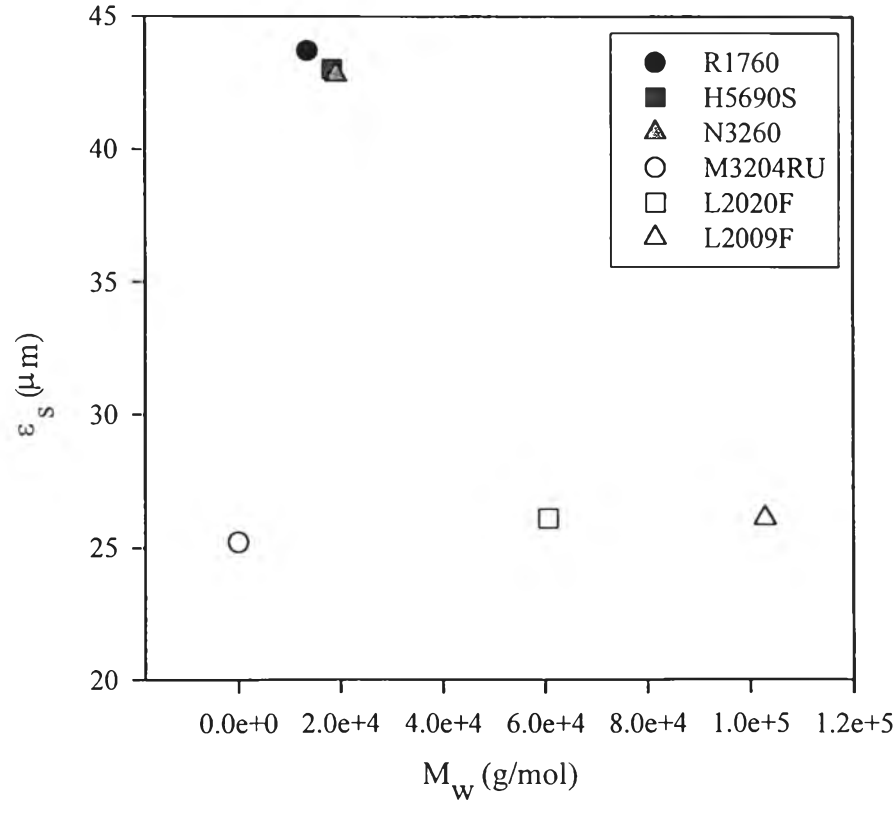
45
40
35
30
25
20
ε_s (μm)
R1760
H5690S
N3260
M3204RU
L2020F
L2009F
0.0e+0
2.0e+4
4.0e+4
6.0e+4
8.0e+4
1.0e+5
1.2e+5
M_w (g/mol)

(b)

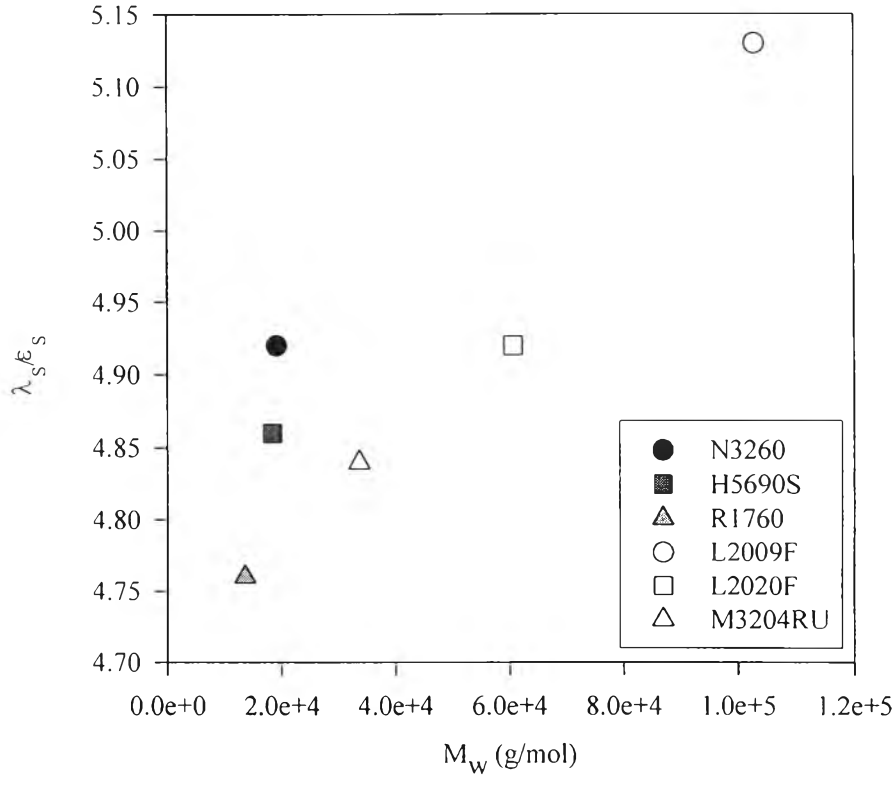

(c)

Figure 3.9 HDPE (N3260, H5690S, R1760) and LLDPE (L2009F, L2020F) and MDPE (M3204RU) at 190 ^{o}C: a) λ_S vs. M_W; b) ε_S vs. M_W; c) λ_S/ε_S vs. M_W.

Figure 3.9 shows a) λ_S vs. M_W; b) ε_S vs. M_W; c) λ_S/ε_S vs. M_W of HDPE (N3260, H5690S, R1760) and LLDPE (L2009F, L2020F) and MDPE (M3204RU). The melt temperature was fixed at 190 ^{o}C. We can see that both the wavelength (λ_S) and the amplitude (ε_S) increase with melt temperature. The mean sharkskin amplitudes are 42.8, 43.0 and 43.7 mm for HDPE (N3260, H5690S, R1760) and 26.1, 26.1 and 25.2 mm for LLDPE (L2009F, L2020F) and MDPE (M3204RU) for the HDPE's with the molecular weights of 1.92×10^4, 1.84×10^4, 1.36×10^4 g/mol and for the LLDPE and MDPE with the molecular weights of 1.03×10^5, 6.07×10^4, 6.07×10^4 g/mol respectively. Similarly, the corresponding sharkskin wavelengths are 211, 208 and 208 mm for HDPE and 133, 129, and 121 mm for LLDPE and MDPE and the sharkskin

ratio are 4.92. 4.83 and 4.75 for HDPE and 5.13, 4.92 and 4.84 for LLDPE and MDPE respectively. The formation of sharkskin extrudates involves chain relaxation during solidification. A HDPE or MDPE with a lower molecular weight favors disturbances of a higher wavenumber or a lower wavelength. The skin relaxations at the die outlet where the sharkskin extrudates originate are faster for an HDPE or MDPE with a lower molecular weight. The apparent reason is shorter chains do not need to reentangle and relaxations can terminate in a shorter period resulting in the shorter wavelength and amplitude.

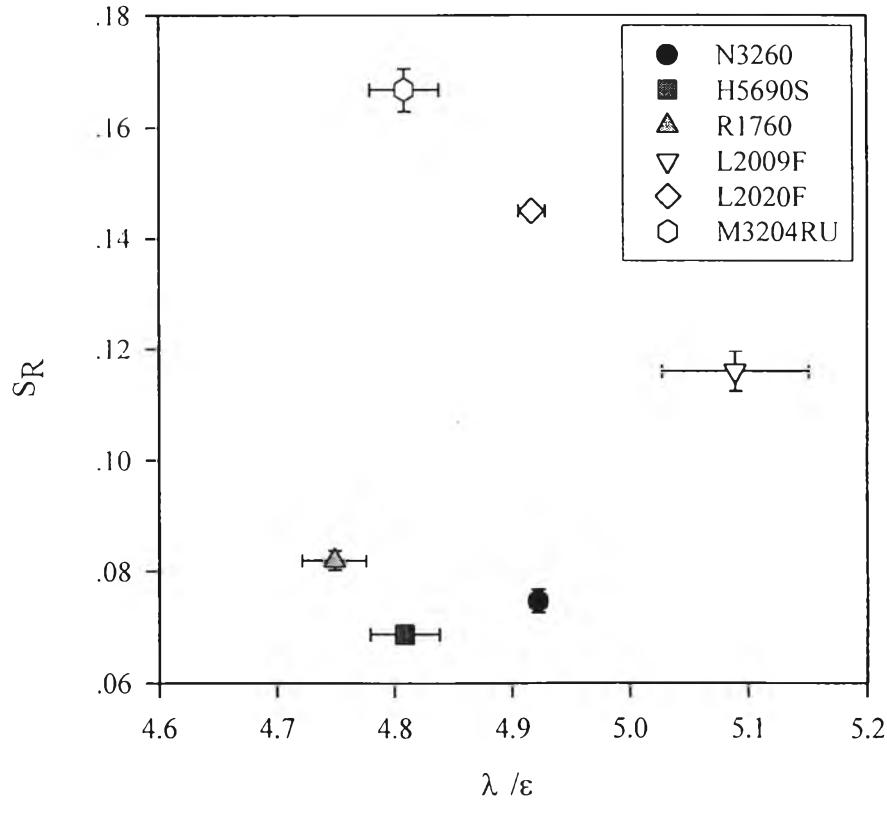

Figure 3.10 Stability diagram between S_R vs. λ_S/ε_S of HDPE (H5690S) and LLDPE (L2020F) at 190 ^oC.

Figure 3.10 shows a stability diagram between S_R vs. λ_S/ε_S of HDPE (H5690S) and LLDPE (L2020F) at 190 ^oC. The recoverable shear was

obtained from the critical wall shear stress divided by the storage modulus. The wavelength is proportional to the amplitude for all materials and the characteristic ratio has a higher value for a higher molecular weight because of greater friction coefficient. When we compare the characteristic ratio S_R between HDPE and LLDPE, we can see that LLDPE and MDPE have high values of the characteristic ratio S_R, we are not sure of reasons for this behavior. It is interesting to note that boundary assumes nearly constant values with respect to the material but independent of molecular weight. The asymptotic recoverable shear depends on the regime or the skin texture type that appears. Therefore, an appearance of each skin texture would require a different level of S_R to initiate a surface texture.

3.4 Effect of temperature on (λ_s, ε_s) of HDPE (H5690S) and LLDPE (L2020F)

Table 3.8 Skin parameters and normalizations for sharkskin defect of HDPE (H5690S) and LLDPE (L2020F) at various temperatures die no. 614

Temperature (°C)	$\tau_{w,c} \times 10^{-6}$ (dynes/cm^2) (avg.)	$G''_N \times 10^{-7}$ (dynes/cm^2)	S_R (avg.)	λ_S (avg.)	ε_S (avg.)	λ_S/ε_S (avg.)
H5690S						
210	2.22	3.44	0.065	135	26.4	5.12
200	2.24	3.37	0.066	130	26.2	4.97
190	2.26	3.30	0.069	129	26.1	4.83
180	2.28	3.23	0.071	121	26.0	4.67
170	2.29	3.16	0.072	117	26.0	4.50
160	2.30	3.09	0.075	112	25.6	4.37
150	2.31	3.01	0.077	108	25.5	4.23
L2020F						
200	2.59	1.84	0.065	214	43.5	4.92
190	2.61	1.80	0.066	208	43.0	4.92
180	2.92	1.76	0.069	194	40.9	4.74
170	3.26	1.72	0.071	185	40.1	4.61
160	3.72	1.68	0.072	180	39.8	4.52

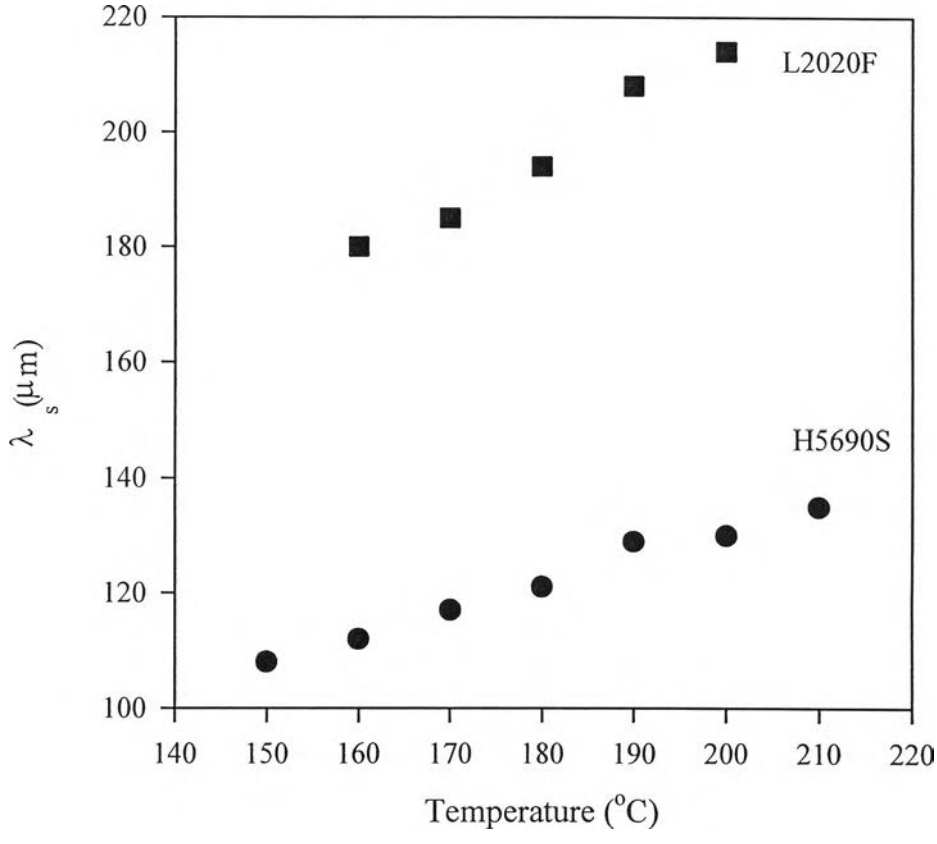
220
200
180
160
140
120
100
λ_s (μm)
L2020F
H5690S
140
150
160
170
180
190
200
210
220
Temperature (°C)

(a)

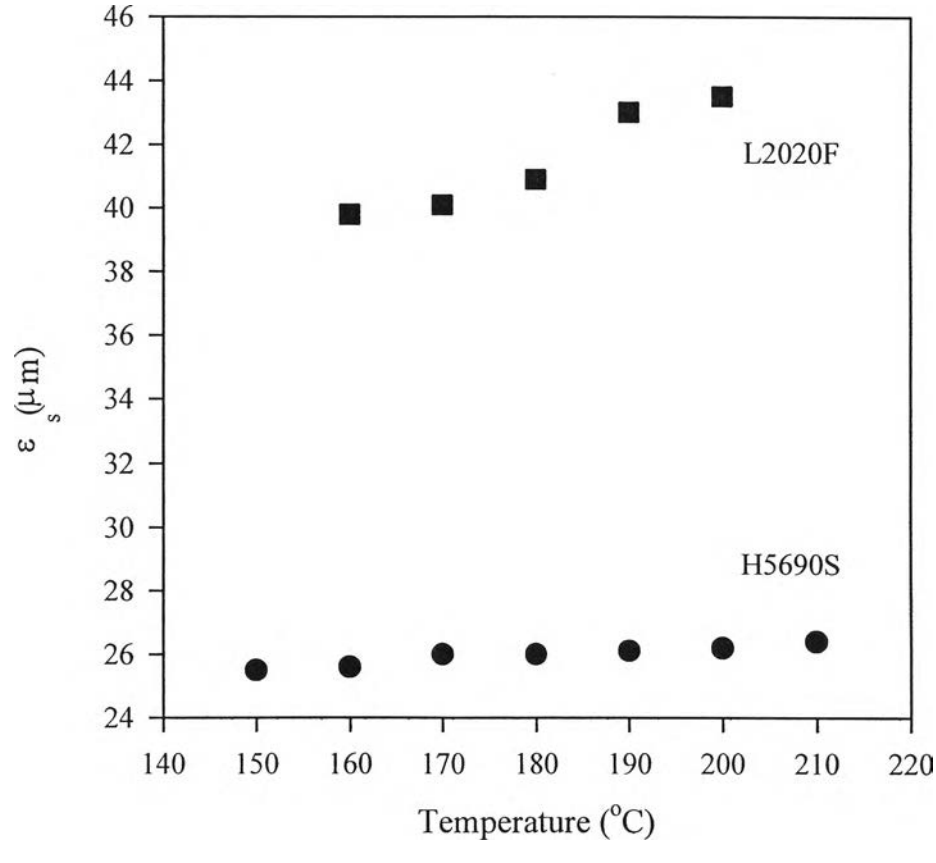
46
44
42
40
38
36
34
32
30
28
26
24
ε_s (μm)
L2020F
H5690S
140
150
160
170
180
190
200
210
220
Temperature (°C)

(b)

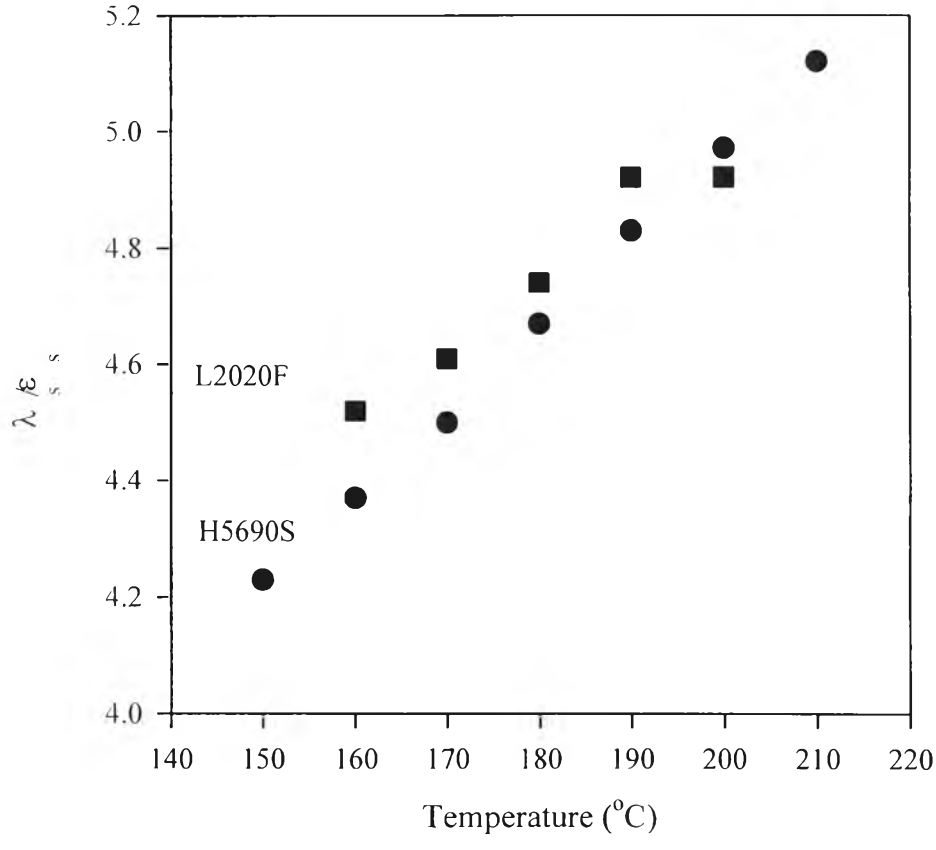

Figure 3.11 HDPE (H5690S) various temperatures (150 °C - 210 °C) and LLDPE (L2020F) various temperatures (160 °C - 200 °C): a) λ_S vs. temperature; b) ε_S vs. temperature; c) λ_S/ε_S vs. temperature.

Figure 3.11 shows a) λ_S vs. temperature; b) ε_S vs. temperature; c) λ_S/ε_S vs. temperature of HDPE (H5690S) at various temperatures (150 °C - 210 °C) and LLDPE (L2020F) at various temperatures (160 °C - 200 °C). The sharkskin wavelength (λ_S) and amplitude (ε_S) both increase with melt temperature. The ratio λ_S/ε_S increases from 4.23 mm to 5.12 mm for HDPE (H5690S) as the melt temperature is raised from 150 °C - 210 °C (the values are tabulated in Table 3.8), and increases from 4.52 mm to 4.92 mm for LLDPE (L2020F) as the melt temperature is raised from 160 °C - 200 °C . When the melt temperature is raised, the melt viscosity decreases and the chain disentanglement becomes dynamically enchanced. A melt confined within a

more severe disentanglement layer tends to relax more slowly, and therefore its sharkskin wavelength and amplitude are expectedly larger. When we compare between HDPE (H5690S) and LLDPE (L2020F) melts we can see that LLDPE melts (L2020F; L 160 °C - L 200 °C) have higher values of λ_s and ε_s than those of HDPE melts (H5690S; H 150 °C - H 210 °C) because it is of a higher molecular weight and therefore it has a higher friction coefficient leading to higher relaxation times.

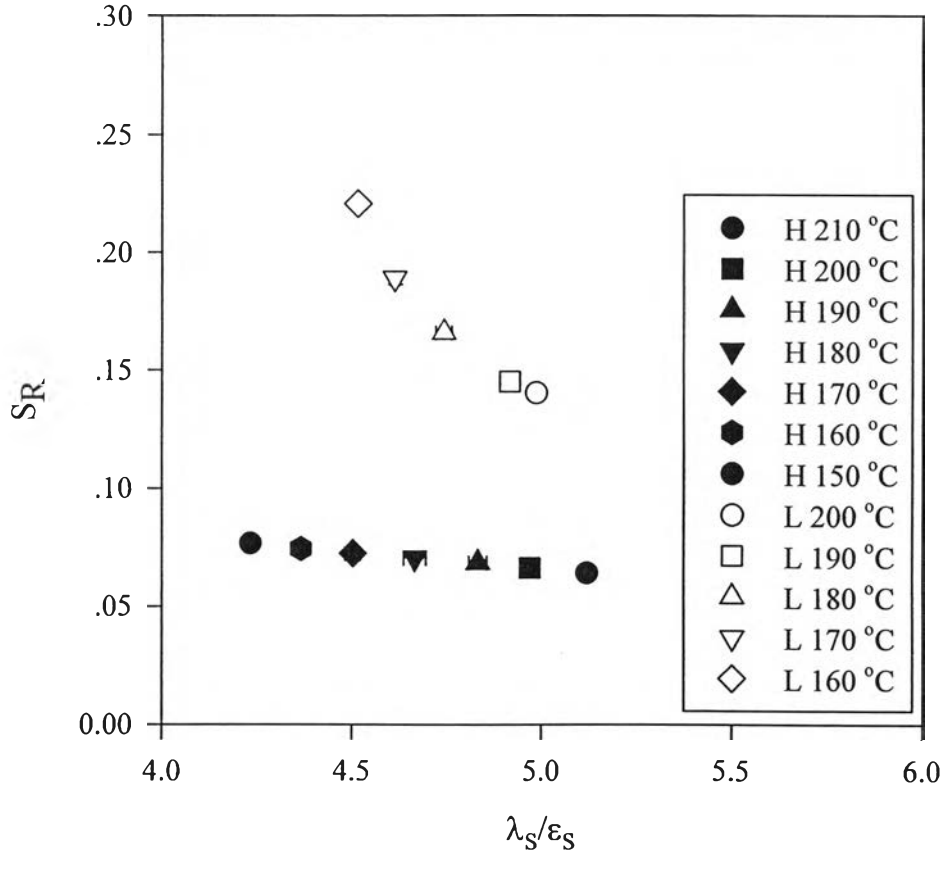

Figure 3.12 Stability diagram of HDPE (H5690S) various temperatures (210 °C - 150 °C) and LLDPE (L2020F) various temperatures (200 °C - 160 °C).

Figure 3.12 shows a stability diagram of HDPE (H5690S) melts at various temperature (210 °C - 150 °C) and LLDPE (L2020F) melts various

temperature (200 ^{o}C - 160 ^{o}C). We conclude that the critical wall shear stress varies inversely with temperature consistent with the published data (*Howells and Benbow, 1962*). G''_N lightly changes with temperature or G''_N is practically independent of temperature; then S_R decreases as temperature increases (the value are tabulated in Figure 3.12). There are boundary lines in the stability diagram: one is for LLDPE (L2020F; T 200 ^{o}C - T 160 ^{o}C) and another is for HDPE (H5690S; T 210 ^{o}C - T 160 ^{o}C).

3.5 Effect of Die Geometry on (λ_s, ε_s) of H5690S and L2020F

Table 3.9 Skin parameters and normalizations of sharkskin defect of LLDPE (L2020F) and HDPE (H5690S) at various diameters used

Die No.	l_c/d_c	$\tau_{w,c}\times10^{-6}$ (dynes/cm^2) (avg.)	$G''_N \times 10^{-7}$ (dynes/cm^2)	S_R (avg.)	λ_s (μm) (avg.)	ε_s (μm) (avg.)	λ_s/ε_s (avg.)
H5690S							
214	7.04	2.61	3.3	0.079	203	41.8	4.86
614	33.4	2.81	3.3	0.085	208	43.4	4.80
1860	40.1	4.04	3.3	0.093	217	47.9	4.53
L2020F							
214	7.04	2.63	1.8	0.145	124	24.3	5.12
614	33.4	2.82	1.8	0.156	128	26.1	4.92
1860	40.1	3.08	1.8	0.171	135	28.0	4.82

Table 3.9 shows λ_S and ε_S as function of d_C. Since λ_S and ε_S increase with d_C, the onset of sharkskin is easier to detect using a larger d_C consistent with published data (*Wang and Drda, 1996*) or we can conclude that both λ_S and ε_S increase with the ratio l_C/d_C ; λ_S's values obtained are 203, 208 and 217

HDPE (H5690S) and 124, 128 and 135 μm for LLDPE (L2020F), and ε_s's values obtained are 41.8, 43.4 and 47.9 μm for HDPE (H5690S) and 24.3, 26.1 and 28.0 μm for LLDPE (L2020F) when l_c/d_c varies from 7.01, 33.4 and 40.1. For a longer die, the melt at the interface is subjected to the same stress level but for a longer duration resulting in a more severe chain disentanglement. The time scale of skin relaxations at the die outlet are therefore greater and hence a longer wavelength. The result are shown in Figure3.13a-c below.

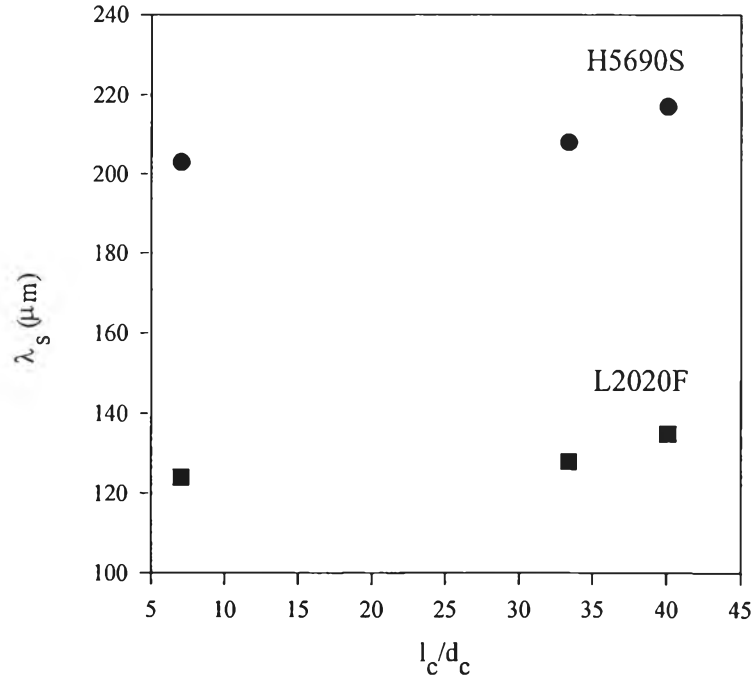

(a)

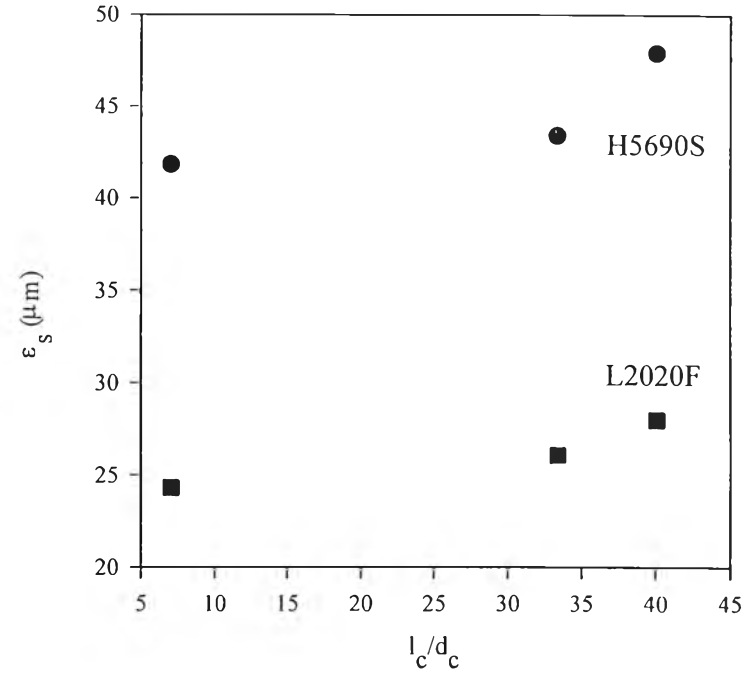

(b)

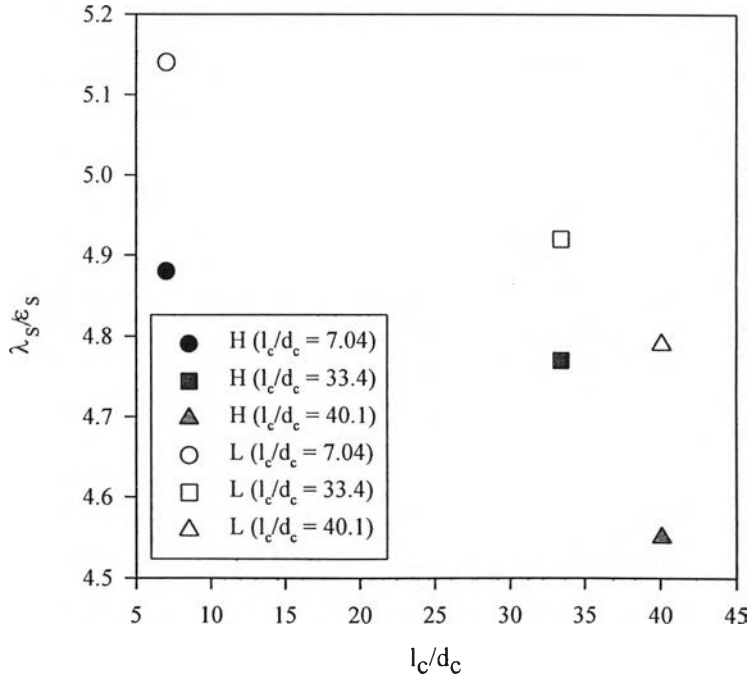

(c)

Figure 3.13 HDPE (H5690S) various die (214, 614 and 1860) and LLDPE (L2020F) various die (214, 614 and 1860): a) λ_S vs. l_c/d_c; b) ε_S vs. l_c/d_c; c) λ_S/ε_S vs. l_c/d_c.

Figures 3.13 shows λ_S/ε_S vs. l_c/d_c of HDPE (H5690S) sharkskin from various dies (214, 614 and 1860) and LLDPE (L2020F) sharkskin from various dies (214, 614 and 1860). The sharkskin parameter λ_S/ε_S decreases from 4.86, 4.80 and 4.53 as the l_c/d_c increases from 7.04 , 33.4 and 40.1 for HDPE (H5690S) and the sharkskin parameter λ_S/ε_S decreases from 5.12, 4.92 and 4.82 as the l_c/d_c increases from 7.04 , 33.4 and 40.1 for LLDPE (L2020F) .

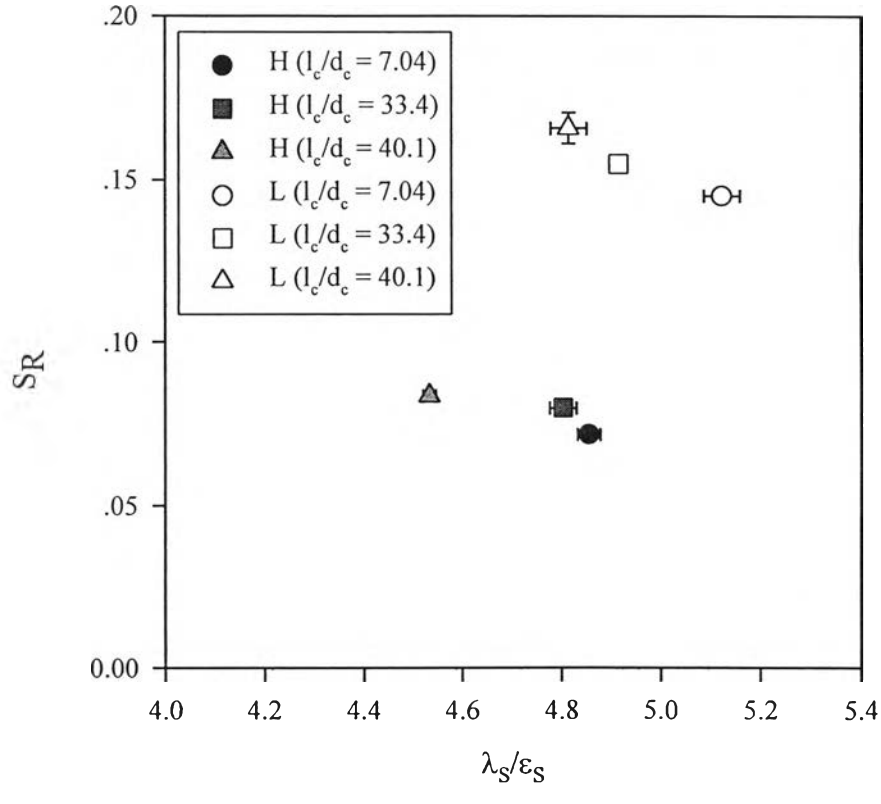

Figure 3.14 A stability diagram of HDPE (H5690S) various die (214, 614 and 1860) and LLDPE (L2020F) various die (214, 614 and 1860).

Figure 3.14 shows a stability diagram of HDPE (H5690S) sharkskin obtained from various dies (214, 614 and 1860) and LLDPE (L2020F) sharkskin obtained various dies (214, 614 and 1860). There are two boundaries; one is for HDPE and another is for LLDPE and MDPE.

3.6 Stability Diagram of HDPE and LLDPE

The Stability diagram of the sharkskin defects is not available in literature, so the proposed the work is original. None of publishes numerical work addressed or linked flow instabilities to the extrudate skin defect. Stability diagram is defined as the separation of regimes in a parameter space; the parameters are generally normalized. So that, if all relevant parameters are accounted for, the stability diagram should be universal. We chosed λ_s/ε_s an a normalized skin parameter where λ_s is the wavelength (the length between the depth) of the sharkskin extrudate and ε_s is the amplitude (the height of the depth) of the sharkskin extrudate.

3.6.1 λ_s/ε_s vs. S_R - Stability Diagrams

Figure 3.15 shows the stability diagram (S_R vs. λ_s/ε_s) of the sharkskin surface of regime II (sharkskin defect). There are two boundaries, one for the three HDPE's and the other one for the LLDPE's and MDPE's. For each type of polymer, when we varied temperature or die geometry the boundary remains the same or collapsed with that when M_w was varied. If we had used other grades of HDPE and LLDPE, we would obtain these two boundaried: one for HDPE's and another for LLDPE's. S_R which characterizes the onset of sharkskins is nearly unique because the onset mechanism is solely material dependent. On the other hand, the sharkskin parameter λ_s/ε_s varies a great deal depending on molecular weight, the melt temperature and die geometry.

The results of all stability diagrams and dependences on molecular weight, melt temperature and die geometry are shown below.

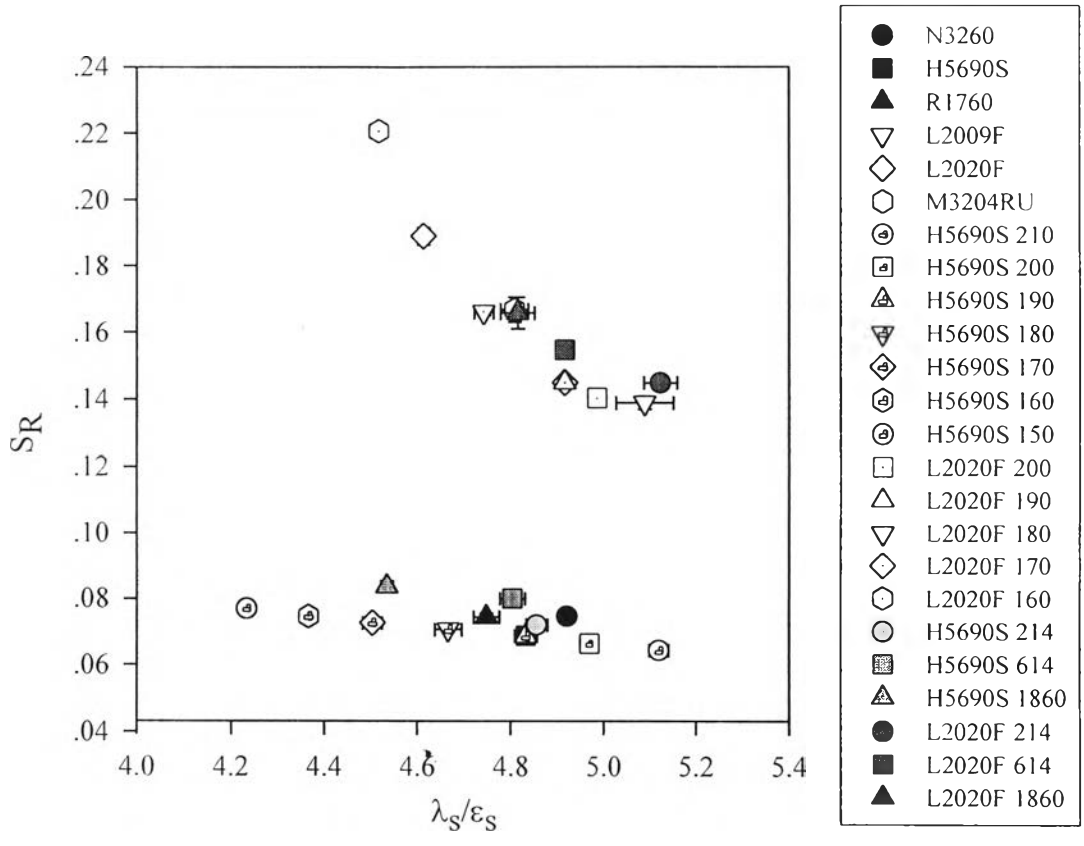

Figure 3.15 Stability diagram of HDPE, LLDPE and MDPE of various materials, melt temperatures and diameter geometry.